

Subcellular localization of *Mycoplasma pneumoniae* proteins visualized by fluorescent protein tagging

Tsuyoshi Kenri,¹ Shintaro Seto,² Atsuko Horino,¹ Yuko Sasaki,¹ Tsuguo Sasaki,¹ and Makoto Miyata³

¹Department of Bacterial Pathogenesis and Infection Control, National Institute of Infectious Diseases, Musashimurayama, Tokyo 208-0011, Japan

²Department of Oral Microbiology, Meikai University School of Dentistry, Saitama 350-0283, Japan

³Department of Biology, Graduate School of Science, Osaka City University, Sumiyoshi-ku, Osaka, 558-8585, Japan; PRESTO, JST, Osaka 558-8585, Japan

ABSTRACT

Subcellular localizations of four *M. pneumoniae* proteins P65, HMW2, P41, and P24 that are encoded in the *crl* operon (for "cytadherence regulatory locus") were visualized by a fluorescent protein-tagging strategy. The P65 and HMW2 proteins fused to enhanced yellow fluorescent protein (EYFP), were observed to localize at the attachment organelle by fluorescence microscopy. On the other hand, the P41 and P24 proteins labeled with EYFP were localized at the proximal end of the attachment organelle. This difference of the localization pattern was more clearly shown by a dual labeling of fluorescent proteins using EYFP and ECFP (enhanced cyan fluorescent protein). The localization of P41 and P24 at the proximal end of the attachment organelle suggested that they are also cytoskeletal proteins that form unknown structures at this site.

INTRODUCTION

Mycoplasma pneumoniae lacks a cell wall but has internal cytoskeleton-like structures that are assumed to support the attachment organelle and asymmetric cell shape of this bacterium. The cytoskeleton-like structures have been observed in electron micrographs of *M. pneumoniae* and are thought to play important roles in cell division, cytadherence and gliding motility (1). The most remarkable architectural feature of the cytoskeleton-like structure is the electron-dense core, a rod-like structure that exists longitudinally at the center of the attachment organelle. This rod-like structure, measuring about 300 nm long and 80 nm thick, has a knob at the distal end (terminal button). A network of fibrous structure is also observed in the cytoplasm of *M. pneumoniae*. Although it is believed that these cytoskeleton-like structures are composed of the cytadherence-related proteins and the other Triton-X100 insoluble proteins, actual components and fine structural detail are poorly understood. In this study, we have developed a dual GFP expression system in *M. pneumoniae* to study the spatial relationship of candidate proteins of the cytoskeleton-like structures.

MATERIALS AND METHODS

Organism and culture conditions. *M. pneumoniae* strains were cultured in PPLO medium (2.1% PPLO broth, 0.25% glucose, 0.002% phenol red, 0.5% yeast extract, 10% horse serum, 50 µg of ampicillin/ml). For drug-resistant *M. pneumoniae* strains, 18

µg of gentamicin/ml or 15 µg of chloramphenicol/ml was added to the media.

Gene transfer. Tn 4001-derivitive vectors, pISM2062.2 and pKV 104 (2, 3) were used to deliver GFP genes into *M. pneumoniae* cells. The genes coding for EYFP and ECFP were introduced into pISM2062.2 and pKV104 vectors, respectively. *M. pneumoniae* genes were amplified by PCR and were connected to the EYFP or ECFP genes.

Microscopy. *M. pneumoniae* cells were observed with a BX51 fluorescence microscope equipped with YFP and CFP filter units and a phase-contrast setup (Olympus). The images were digitized by using a Photometrics CoolSNAPcf charge-coupled device camera (Roper Scientific).

RESULTS AND DISCUSSION

The *p65*, *hmw2*, *p41* and *p24* genes were cloned and connected to 3' end of *eyfp* gene on the plasmid pISM2062.2 and introduced into *M. pneumoniae* cells. The *M. pneumoniae* cells transformed with each of these plasmids expressed EYFP-P65, EYFP-HMW2, EYFP-P41 and EYFP-P24 fusion proteins. Subcellular localizations of these fusion proteins were examined by fluorescence microscopy. The EYFP-P65 and EYFP-HMW2 proteins were localized at the attachment organelle, supporting the results of the other reports (4,5). P65 and HMW2 are thought to be the components of the attachment organelle. On the other hand, EYFP-P41 and EYFP-P24 were localized at the proximal

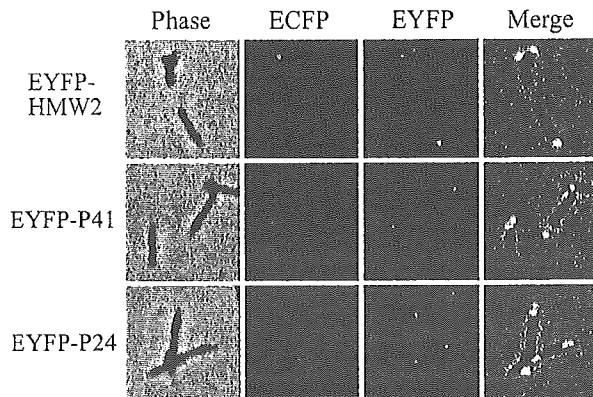


Fig. 1. Subcellular localization of ECFP-P65, EYFP-HMW2, EYFP-P41, and EYFP-P24 fusions in the *M. pneumoniae* cells. Images of three *M. pneumoniae* transformants are shown. The EYFP fusion indicated at the left is expressed in the strain. Three strains also express ECFP-P65 fusion. The first panel in each row shows the phase-contrast image of the cells. The second and third panels in each row show ECFP and EYFP fluorescence images of the same cells, respectively. The fourth panel in each row shows the merged image of the phase-contrast and fluorescence images.

end of the attachment organelle. This position is thought to correspond to the proximal end of the rod-like structure. We then coexpressed an ECFP-P65 protein with the EYFP-HMW2, EYFP-P41 or EYFP-P24 proteins by using the pKV104 vector. These experiments clearly showed that P65 and HMW2 are present at the attachment organelle, but P41 and P24 are at the proximal end the attachment organelle (Fig. 1). The clear localization P41 and P24 strongly suggested that these proteins are also cytoskeletal proteins. Recently, the presence of a wheel-like complex that might be part of a cytoskeleton-like structure was suggested at the proximal end of the electron-dense core by transmission electron microscopy of an ultrathin section of *M. pneumoniae* cells (6). Although the detailed structure of this complex is not yet elucidated, it is possible that P41 and P24 are

related to this structure. The dual GFP labeling method we have developed in this study (7) may serve as a powerful tool for identifying components of the attachment organelle and cytoskeleton-like structures.

REFERENCES

1. Krause, D. C., M. F. Balish, S. M. Ross, and M. Fisseha 2004. Cellular engineering in a minimal microbe: structure and assembly of the terminal organelle of *Mycoplasma pneumoniae* Mol Microbiol. **51**: 917-924.
2. Knudtson, K. L., and F. C. Minion 1993. Construction of Tn 4001 lac derivatives to be used as promoter probe vectors in mycoplasmas. Gene. **137**: 217-222.
3. Hahn, T. W., E. A. Mothershed, R. H. Waldo, and D. C. Krause 1999. Construction and analysis of a modified Tn 4001 conferring chloramphenicol resistance in *Mycoplasma pneumoniae*. Plasmid. **41**: 120-124.
4. Seto, S., G. Layh-Schmitt, T. Kenri, and M. Miyata 2001. Visualization of the attachment organelle and cytodherence proteins of *Mycoplasma pneumoniae* by immunofluorescence microscopy. J. Bacteriol. **183**: 1621-1630.
5. Balish, M. F., R. T. Santurri, A. M. Ricci, K. K. Lee, and D. C. Krause 2003. Localization of *Mycoplasma pneumoniae* cytodherence-associated protein HMW2 by fusion with green fluorescent protein: implications for attachment organelle structure. Mol. Microbiol. **47**: 49-60.
6. Mayer, F. 2003. Cytoskeletons in prokaryotes Cell Biol. Int. **27**: 429-438.
7. Kenri, T., S. Seto, A. Horino, Y. Sasaki, T. Sasaki, and M. Miyata 2004. Use of fluorescent-protein tagging to determine the subcellular localization of *Mycoplasma pneumoniae* proteins encoded by the cytodherence regulatory locus J. Bacteriol. **186**: 6944-6955.

Typing analysis of clinical isolates of *Mycoplasma pneumoniae* in Japan

Tsuyoshi Kenri¹, Norio Okazaki², Mitsuo Narita³ and Tsuguo Sasaki¹

1:Dept. of Bacterial Pathogenesis and Infect Control, Natl Inst of Infect Disease, Japan

2:Kanagawa Prefectural Public Health Laboratory, Chigasaki, Japan

3:JR Sapporo Tetsudo Hospital, Sapporo, Japan

Seventy eight *M. pneumoniae* strains collected in Japan during 1995 and 2003 were genotyped based on nucleotide sequence polymorphism of the *p1* gene. This genotyping established that 26 of the isolates were group I, 45 were group II, and 7 were the variant of group II. The annual occurrence of these isolates showed a dominance of group II between 1995 and 2001. Group I strain was not found in this period. However, group I strains were appeared in 2002 and were dominated in 2003 (67% of total isolates, n=36). We also analyzed the type of the *p1* gene DNA detected from throat swabs and expectorations of patients of respiratory infection. This showed that the appearance pattern of the two groups was similar to that of clinical isolates in this period. These genotyping results indicated that the type of the prevalent clinical strain of *M. pneumoniae* in Japan changed from group II to group I between 2001 and 2003.

INTRODUCTION

M. pneumoniae strains can be classified into two groups (group I and II) based on a nucleotide sequence polymorphism of the *p1* gene that encodes major adhesin protein. In this classification system, the standard laboratory strain M129 is classified into group I and the FH is group II. We previously classified 215 *M. pneumoniae* clinical strains isolated from pneumonia and bronchitis patients in Japan between 1976 and 1994 and reported the alternate increase of group I and group II isolates at the intervals of several years (1). It is well known that outbreaks of mycoplasma pneumonia occur periodically at the intervals of 3 to 7 years, although the reason of this phenomenon is not known. So it is of interest to investigate whether there are correlations between the type shift of *M. pneumoniae* clinical isolates and the periodical pneumonia outbreaks.

We report here the genotyping results of the *M. pneumoniae* clinical isolates and *p1* gene DNA amplified from clinical specimens between 1995 and 2003.

MATERIALS AND METHODS

M. pneumoniae strains were isolated independently from pneumonia patients during 1995 and 2003 in three areas of Japan. These *M. pneumoniae* strains were cultured in PPLO medium at 37°C and were filter-cloned before the genotyping analysis was performed. Genotyping of *M. pneumoniae* clinical isolates was performed by the PCR-RFLP method as described previously (2, 3). Throat swabs were collected from 89 patients of primary atypical pneumonia or bronchitis. Expectorations were collected from 925 patients suspected of respiratory infections. Detection and genotyping of *p1* genes from these clinical specimens were

done by the PCR-based method using specific primers.

RESULTS AND DISCUSSION

The genotyping results were summarized in the Table 1. The results revealed that there were no group I isolates between 1995 and 2001. Thirty five isolates were group II and two were the variant of group II in this period. On the other hand, group I strains were found within the isolates of 2002 and 2003. In 2002, two isolates out of five were group I (40%). The isolation rate of group I strain increased apparently in 2003. Twenty four out of 36 strains (67%) were group I in 2003 (Table 1A). We also analyzed 89 throat swabs collected from pneumonia and bronchitis patients during the period of 1995 to 2000 and 925 expectoration samples collected from patients suspected of respiratory infection during 2000 to 2003. The *p1* genes were detected from 24 specimens of throat swabs (27%) and were genotyped by the PCR-RFLP method. This established that the all of the *p1* genes detected from throat swabs were group II (Table 1B). The expectorations were analyzed by a nested PCR method that amplifies the RepMP4 region of the *p1* gene. The *p1* gene was detected from 91 out of 925 expectorations (9.8%) by the method and 81 of these were typable (Table 3C). In this analysis, group I *p1* genes were found only in the specimens after 2001. These typing results strongly suggested that type of prevalent clinical *M. pneumoniae* strain has changed recently in Japan from group II to group I. The Fig. 1 shows that the weekly cases of mycoplasma pneumonia in Japan. The pneumonia cases tend to increase after 2000. There is a possibility that the type shift phenomenon of clinical strains is involved in the increase of pneumonia cases.

Table 1. Genotyping results of *M. pneumoniae* in clinical samples.

Clinical isolats									
	1995	1996	1997	1998	1999	2000	2001	2002	2003
Group I	0	0	0	0	0	0	0	2 ^b	24
Group II	7	13	2	5	0	2	6	3	7
II variant	0	0	0	1	0	0	1	0	5

B. Throat swabs

	1997	1998	1999	2000
Group I	0	0	0	0
Group II	6	4	1	13

C. Expectorations

	2000	2001	2002	2003
Group I	0	14	24	2
Group II	9	13	19	0

REFERENCES

1. Sasaki, T., T. Kenri, N. Okazaki, M. Iseki, R. Yamashita, M. Shintani, Y. Sasaki, and M. Yayoshi 1996. Epidemiological study of *Mycoplasma pneumoniae* infections in Japan based on PCR-restriction fragment length polymorphism of the P1 cytoadhesin gene. *J. Clin. Microbiol.* **34**: 447-449.
2. Kenri, T., R. Taniguchi, Y. Sasaki, N. Okazaki, M. Narita, K. Izumikawa, M. Umetsu, and T. Sasaki 1999. Identification of a new variable sequence in the P1

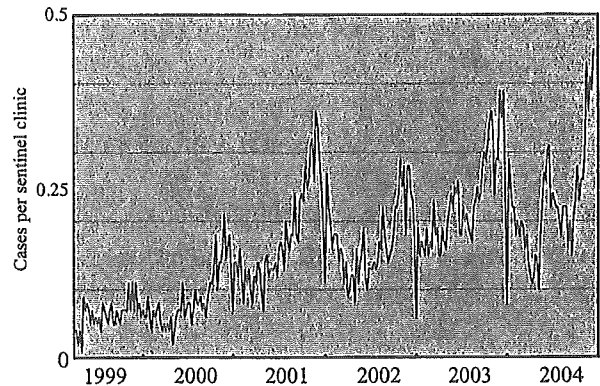


Fig. 1. Weekly cases of mycoplasma pneumonia in Japan. (Infectious disease surveillance center, National Institute of Infectious Diseases)

cytoadhesin gene of *Mycoplasma pneumoniae*: evidence for the generation of antigenic variation by DNA recombination between repetitive sequences. *Infect. Immun.* **67**: 4557-4562.

3. Cousin-Allery, A., A. Charron, B. de Barbeyrac, G. Fremy, J. Skov Jensen, H. Renaudin, and C. Bebear 2000. Molecular typing of *Mycoplasma pneumoniae* strains by PCR-based methods and pulsed-field gel electrophoresis. Application to French and Danish isolates. *Epidemiol. Infect.* **124**: 103-111.

Use of Fluorescent-Protein Tagging To Determine the Subcellular Localization of *Mycoplasma pneumoniae* Proteins Encoded by the Cytadherence Regulatory Locus

Tsuyoshi Kenri,^{1*} Shintaro Seto,^{2†} Atsuko Horino,¹ Yuko Sasaki,¹
Tsuguo Sasaki,¹ and Makoto Miyata^{2,3}

Department of Bacterial Pathogenesis and Infection Control, National Institute of Infectious Diseases, Musashimurayama, Tokyo,¹ and Department of Biology, Graduate School of Science, Osaka City University,² and PRESTO, JST,³ Sumiyoshi-ku, Osaka, Japan

Received 13 May 2004/Accepted 15 July 2004

Mycoplasma pneumoniae lacks a cell wall but has internal cytoskeleton-like structures that are assumed to support the attachment organelle and asymmetric cell shape of this bacterium. To explore the fine details of the attachment organelle and the cytoskeleton-like structures, a fluorescent-protein tagging technique was applied to visualize the protein components of these structures. The focus was on the four proteins—P65, HMW2, P41, and P24—that are encoded in the *crl* operon (for “cytadherence regulatory locus”), which is known to be essential for the adherence of *M. pneumoniae* to host cells. When the P65 and HMW2 proteins were fused to enhanced yellow fluorescent protein (EYFP), a variant of green fluorescent protein, the fused proteins became localized at the attachment organelle, enabling visualization of the organelles of living cells by fluorescence microscopy. The leading end of gliding *M. pneumoniae* cells, expressing the EYFP-P65 fusion, was observed as a focus of fluorescence. On the other hand, when the P41 and P24 proteins were labeled with EYFP, the fluorescence signals of these proteins were observed at the proximal end of the attachment organelle. Coexpression of the P65 protein labeled with enhanced cyan fluorescent protein clearly showed that the sites of localization of P41 and P24 did not overlap that of P65. The localization of P41 and P24 suggested that they are also cytoskeletal proteins that function in the formation of unknown structures at the proximal end of the attachment organelle. The fluorescent-protein fusion technique may serve as a powerful tool for identifying components of cytoskeleton-like structures and the attachment organelle. It can also be used to analyze their assembly.

Mycoplasma pneumoniae, one of the smallest self-replicating bacteria known, is a causative agent of bronchitis and primary atypical pneumonia in humans (43, 44). *M. pneumoniae* lacks a cell wall and hence has a pleomorphic cell shape. However, a majority of *M. pneumoniae* cells in cultures are filamentous and have a differentiated terminal structure at one pole. This terminal structure, the attachment organelle, is a tapered membrane protrusion responsible for the adherence of *M. pneumoniae* to host respiratory epithelium (cytadherence) (23, 24). The attachment organelle renders *M. pneumoniae* cells asymmetric and functions as a leading end for gliding motility. This organelle also may have a role in initiating cell division in *M. pneumoniae*, because the bifurcation of the attachment organelle seems to occur prior to the binary fission of *M. pneumoniae* (2, 6, 7, 25, 26, 34, 36, 48).

The attachment organelle and polar filamentous cell shape of *M. pneumoniae* are thought to be stabilized by intracellular cytoskeleton-like structures, which have been observed in electron micrographs of *M. pneumoniae* (5, 25, 33). The most remarkable architectural feature of the cytoskeleton-like structures is the electron-dense core, a rod-like structure that exists

longitudinally at the center of the attachment organelle (33). This rod-like structure, measuring about 300 nm long and 80 nm thick, has a knob at the distal end (terminal button) (33, 45). A network of fibrous structures is also observed in the cytoplasm of *M. pneumoniae* (33). These cytoskeleton-like structures are major components of the Triton X-100-insoluble fraction of *M. pneumoniae* cells (Triton shell) and are thought to have a scaffold-like function upon which other cell components construct *M. pneumoniae* cells (45, 51).

A recent report indicated that the Triton X-100-insoluble fraction contains about 100 proteins, including most of the known proteins required for cytadherence (P1, B, C, HMW1, HMW2, and HMW3) (45). These cytadherence-related proteins are believed to be the main components of the attachment organelle and are encoded in three operons, designated *p1*, *hmw*, and *crl*, in the genome (24, 25). Protein P1 (encoded in the *p1* operon) is a major adhesin molecule responsible for cytadherence and is densely clustered at the surface of the attachment organelle (9, 18, 26, 48). Proteins B, C, HMW1, HMW2, and HMW3, called cytadherence accessory proteins, are not adhesin molecules but are required for the formation of functional attachment organelles (2, 3, 25). Proteins B and C, also named P90 and P40 (2, 26), are products of open reading frame 6, which exists just downstream of the *p1* gene in the *p1* operon (19). Proteins B and C associate with protein P1 at the attachment organelle and may support the proper structural configuration of P1 (29, 30). HMW1, HMW2, and HMW3 are large proteins necessary for the localization of P1

* Corresponding author. Mailing address: Department of Bacterial Pathogenesis and Infection Control, National Institute of Infectious Diseases, 4-7-1 Gakuen, Musashimurayama, Tokyo 208-0011, Japan. Phone: 81-42-561-0771. Fax: 81-42-565-3315. E-mail: kenri@nih.go.jp.

† Present address: Department of Oral Microbiology, Meikai University School of Dentistry, 1-1 Keyakidai, Sakado, Saitama 350-0283, Japan.

at the attachment organelle. These HMW proteins are present in high concentrations at the attachment organelle and are thought to be the most likely components of the electron-dense core (3, 25, 48, 49, 52). HMW1 and HMW3 are encoded in the *hmw* operon, and the gene encoding HMW2 is in the *crl* operon (24). In addition to these cytoadherence-related proteins, the Triton X-100-insoluble fraction contains proteins P65 and P200. P65 and P200 share a structural domain, the acidic proline-rich domain, with HMW1 and HMW3 (40, 41). The structural similarity suggests that proteins P65 and P200 have roles similar to those of HMW1 and HMW3 as components of cytoskeleton-like structures. However, it is not clear whether proteins P65 and P200 participate in cytoadherence. Recent studies revealed that P65 localizes to the attachment organelle with P30, an additional adhesin protein that is an essential factor for cytoadherence (2, 20, 25, 48, 49). The genes encoding P65 and P30 are located in the *crl* and *hmw* operons, respectively. The gene encoding P200 is not located in one of the three operons of cytoadherence-related proteins (2, 24).

Although these candidate components of the attachment organelle and cytoskeleton-like structures have been identified, the spatial configuration and interaction between these proteins are poorly understood. Antibodies have been used to localize specific proteins to the attachment organelle (46, 48, 49, 52), but their use is limited because of the need for specificity of an antibody for a target protein and the inability to observe living systems in real time. Green fluorescent protein (GFP), an intrinsically fluorescent molecule obtained from the jellyfish *Aequorea victoria*, is widely used to study protein-protein interactions, cell division, and gene expression in a variety of organisms in real time (39, 50). In this study, we developed a dual GFP expression system for *M. pneumoniae* to study the spatial relationship of P65 to HMW2, P41, and P24, which are encoded in the *crl* operon (28).

MATERIALS AND METHODS

Organism and culture conditions. The *M. pneumoniae* strains listed in Table 1 were cultured in PPLO medium (2.1% PPLO broth [Becton Dickinson, Sparks, Md.], 0.25% glucose, 0.002% phenol red, 0.5% yeast extract [Becton Dickinson], 10% horse serum [Gibco BRL, Rockville, Md.], 50 µg of ampicillin/ml) or in Aluotto medium (1, 38) at 37°C. For drug-resistant *M. pneumoniae* strains, 18 µg of gentamicin/ml or 15 µg of chloramphenicol/ml was added to the media. *Escherichia coli* JM83 (53), DH5α (13), and DB3.1 (Invitrogen, Carlsbad, Calif.) were used as host strains to construct plasmids and were grown in Luria-Bertani medium (47) with or without 50 µg of ampicillin/ml, 50 µg of kanamycin/ml, and 15 µg of chloramphenicol/ml at 37°C.

Construction of fusion genes and plasmids. The synthetic oligonucleotides used for plasmid construction are listed in Table 2. *M. pneumoniae* M129 genomic DNA was prepared by a conventional phenol extraction method. The *p65* gene was amplified from the genomic DNA by PCR with primers P65F-Bam and P65R-Nco. To minimize mutations caused by PCR amplification, high-fidelity DNA polymerase PyroBest (Takara, Tokyo, Japan) was used. The amplified fragment was digested with BamHI and NcoI and was inserted into the BamHI-NcoI site (the 5' end of the *eyfp* gene) of plasmid pEYFP (Clontech, Palo Alto, Calif.), producing a plasmid that we designated pTK150. The *p65* gene was also amplified from the genomic DNA by PCR with primers P65F-Bsr and P65R-Eco. The amplified fragment was inserted into the BsrGI-EcoRI site (the 3' end of the *eyfp* gene) of plasmid pEYFP after digestion with BsrGI and EcoRI, producing a plasmid that we designated pTK153. The *p65-eyfp* and *eyfp-p65* fusion genes were excised from plasmids pTK150 and pTK153 by using PvuII and StuI and were inserted into the SmaI site of plasmid pISM2062.2 (22), producing plasmids pTK155 and pTK158, respectively (Table 3). Plasmids pTK161 and pTK162 (Table 3) were constructed by replacing the *E. coli lac* promoter sequence in pTK158 (derived from plasmid pEYFP) with *p65* or *tuf* promoter

TABLE 1. *M. pneumoniae* strains used in this study^a

Strain	Description ^b
M129	Wild type
TK2062	M129(pISM2062.2)
TK155	M129(pTK155)
TK161	M129(pTK161)
TK162	M129(pTK162)
TK164	M129(pTK164)
TK165	M129(pTK165)
TK210	M129(pTK210)
TK2100	TK210(pISM2062.2)
TK2310	TK210(pMPN310)
TK2311	TK210(pMPN311)
TK2312	TK210(pMPN312)
TK2310T	TK210(pMPN310-tuf)
TK2311T	TK210(pMPN311-tuf)
TK2312T	TK210(pMPN312-tuf)
TK3310	M129(pMPN310)
TK3311	M129(pMPN311)
TK3312	M129(pMPN312)
TK3310T	M129(pMPN310-tuf)
TK3311T	M129(pMPN311-tuf)
TK3312T	M129(pMPN312-tuf)

^a All strains were designed in this study, except for the wild-type strain (31).

^b Tn4001 plasmids were used to transform *M. pneumoniae*.

fragments from *M. pneumoniae* at the BamHI-NcoI site. The *p65* and *tuf* promoter fragments were obtained from *M. pneumoniae* genomic DNA by PCR with primers P65F-Bam and P65-PR and primers tuf-PF and tuf-PR, respectively. These promoter fragments were also used to replace the *p65* gene and its promoter sequence in pTK155 at the BamHI-NcoI site. The resulting plasmids, which expressed the *eyfp* gene alone from the *p65* and *tuf* promoters, were designated pTK164 and pTK165, respectively (Table 3).

The *ecfp* gene was amplified from plasmid pECFP (Clontech) by PCR with primers CFP1F-Sma and CFP-R. The amplified *ecfp* fragment was inserted into the SmaI site of pKV104, producing a plasmid that we designated pTK205. pKV104 contains a chloramphenicol-resistant (Cm^r) variant of Tn4001 (12) and was kindly provided by D. C. Krause of the University of Georgia. The *lac* promoter region of pTK205 (upstream of the *ecfp* gene) was replaced at the SmaI-AgeI site with the *M. pneumoniae tuf* promoter sequence amplified by PCR with primers tuf-F and tufR-Age, resulting in plasmid pTK207. The BsrGI site of pTK207 (the 3' end of the *ecfp* gene) was converted to an EcoRV site with an oligonucleotide linker, 160RVS. Next, the Gateway vector conversion system (reading frame cassette A) (Invitrogen) was inserted into the EcoRV site, producing a plasmid that we designated pTK207-D. The *p65* gene was amplified from *M. pneumoniae* genomic DNA with primers MPN309-F-Gw and MPN309-R-Gw, subcloned into plasmid pDONR201 (Invitrogen) by using BP clonease (Invitrogen), and then transferred to plasmid pTK207-D by using LR clonease (Invitrogen); this procedure produced plasmid pTK210 (Table 3).

Plasmids containing *hmw2*, *p41*, and *p24* fusion genes were constructed as follows. The BsrGI site of plasmid pTK164 and that of plasmid pTK165 were converted to an EcoRV site by inserting an oligonucleotide linker, 160RVS. Next, the Gateway vector conversion system (reading frame cassette A) was inserted into the created EcoRV site, producing plasmids pTK164-D and pTK165-D. The *hmw2* gene sequence was amplified from *M. pneumoniae* genomic DNA by PCR with primers MPN310-F-Not and MPN310-R-Asc. After digestion with NotI and AscI, the *hmw2* gene fragment was inserted into the NotI-AscI site of plasmid pENTR/D-TOPO (Invitrogen), resulting in a plasmid that we designated pMPN310-E. The *p41* and *p24* gene sequences were amplified from *M. pneumoniae* genomic DNA by PCR with primers MPN311-F-Gw and MPN311-R-Gw and primers MPN312-F-Gw and MPN312-R-Gw, respectively. The amplified fragments were subcloned into plasmid pDONR201 by using BP clonease, producing plasmids that we designated pMPN311-E and pMPN312-E. The *hmw2*, *p41*, and *p24* gene fragments of plasmids pMPN310-E, pMPN311-E, and pMPN312-E were transferred to plasmids pTK164-D and pTK165-D by using LR clonease. The resulting plasmids (pMPN and pMPN-tuf series), which are listed in Table 3, were used to transform *M. pneumoniae*.

Transformation of *M. pneumoniae*. *M. pneumoniae* with the modified Tn4001 (Tn4001mod) plasmids was transformed by the electroporation method described by Hedreyda et al. (15). The transformed cells were grown in liquid PPLO medium containing 18 µg of gentamicin/ml or 15 µg of chloramphenicol/

TABLE 2. Synthetic oligonucleotides used in this study

Oligonucleotide	Sequence ^a
P65F-Bam.....	GCGGGATCCTGCAGCAGCTGACAACAACATTTAGCACACT
P65R-Nco.....	CTAGCCATGGCTTCGTAATAATTCATCACCAC
P65F-Bsr.....	GAGCTGTACAAGATGGATATAAATAAACCCAGG
P65R-Eco.....	TCGCGGAATTCAGCTGTTTATTCGTAATAATTCATCACCAC
P65-PR.....	CAACCCATGGCATTATATCCATTTACTGTCT
tuf-PF.....	GTGGGATCCATTTTGCAAACCTGATGACAA
tuf-PR.....	TAACCCATGGGTTTAGATCGGTCAAATTT
CFP1F-Sma.....	GATCCCCTGGGAGCGCCCAATACGCAAACCGCC
CFP-R.....	CCTATTATTTTGACACCAGAC
165RVS.....	GTACGATATC
tuf-F.....	ATTTTGCAAACCTGATGACAA
tufR-Age.....	TCGGACCGGTTTCTCTCTTGCCATGTGTTTG
MPN309-F-Gw.....	GGGGACAAGTTTGTACAAAAAAGCAGGCTTCATGGATATAAATAAACCCAGGTTGAA
MPN309-R-Gw.....	GGGGACCACTTTGTACAAGAAAGCTGGGTATTATTTCGTAATAATTCATCACCAC
MPN310-F-Not.....	CCGCGGCCGCATGAATGATACTGACAAGAAGT
MPN310-R-Asc.....	GTCGGCGCGCCCTTATTAGCTGCTTTTGGGC
MPN311-F-Gw.....	GGGGACAAGTTTGTACAAAAAAGCAGGCTTCATGACTAATGATTACCAACAATTA
MPN311-R-Gw.....	GGGGACCACTTTGTACAAGAAAGCTGGGTATCCTTCATTACTTTGTTCT
MPN312-F-Gw.....	GGGGACAAGTTTGTACAAAAAAGCAGGCTTCATGAAGGATAGTGACTAACACT
MPN312-R-Gw.....	GGGGACCACTTTGTACAAGAAAGCTGGGTACTTCTTGTAAAGAAATTAAC

^a Recognition sites for restriction enzymes and the *att* sites for recombinase are underlined.

ml. The transformation efficiencies were checked by counting the transformant colonies on PPLO agar plates. To minimize the positional effect of Tn4001 insertion in the comparisons of the transformants, we analyzed and compared the transformant strains as a whole transformed population without picking up a single colony.

Protein analysis. *M. pneumoniae* cells were grown in tissue culture flasks to the mid-log phase and were scraped from the bottom of the flasks. The cells were collected by centrifugation at 20,000 × *g* for 15 min at 4°C and washed three times with phosphate-buffered saline. The final cell suspension, adjusted to a total protein concentration of 1 μg/μl, was lysed by adding sample loading buffer and was subjected to sodium dodecyl sulfate (SDS)-polyacrylamide gel electrophoresis (PAGE) at a load of 5 or 10 μg of total protein per lane (47). For Western blot analysis, the separated proteins were transferred to a nitrocellulose

membrane (Bio-Rad, Hercules, Calif.). Monoclonal antibody JL-8 (specific for *A. victoria* GFP variants) (Clontech) was used at a 1:2,000 dilution to detect enhanced yellow fluorescent protein (EYFP) and enhanced cyan fluorescent protein (ECFP). Anti-P65 antiserum (49) was also used at a 1:2,000 dilution. The reacting antibodies were detected with an alkaline phosphatase-conjugated second antibody (goat anti-mouse immunoglobulin G) (Promega, Madison, Wis.) and 5-bromo-4-chloro-3-indolylphosphate (BCIP)-nitroblue tetrazolium (NBT) color development substrate (Promega) according to manufacturer instructions.

Microscopy. *M. pneumoniae* strains were cultured in Aluotto medium at 37°C to the mid-log phase. Cytadherence-positive cells were scraped from the bottom of the culture flasks after the medium was replaced with a volume of fresh medium that was two to five times smaller. The cell suspension was passed through a 25-gauge needle several times, filtered through a membrane filter unit

TABLE 3. Plasmids constructed in this study^a

Plasmid	Vector	Marker	Promoter	Gene	Expression ^b	Fluorescence ^c	Localization ^d
pTK150	pEYFP	Ap ^r	<i>p65</i>	<i>p65-eyfp</i>	NT	NT	NT
pTK153	pEYFP	Ap ^r	<i>lac (E. coli)</i>	<i>eyfp-p65</i>	NT	NT	NT
pTK155	pISM2062.2	Ap ^r Gm ^r	<i>p65</i>	<i>p65-eyfp</i>	+	+	+
pTK158	pISM2062.2	Ap ^r Gm ^r	<i>lac (E. coli)</i>	<i>eyfp-p65</i>	–	–	–
pTK161	pISM2062.2	Ap ^r Gm ^r	<i>p65</i>	<i>eyfp-p65</i>	+	+	+
pTK162	pISM2062.2	Ap ^r Gm ^r	<i>tuf</i>	<i>eyfp-p65</i>	++	++	+
pTK164	pISM2062.2	Ap ^r Gm ^r	<i>p65</i>	<i>eyfp</i>	+	+	–
pTK164-D	pISM2062.2	Ap ^r Gm ^r Cm ^r	<i>p65</i>	<i>eyfp</i>	NT	NT	NT
pTK165	pISM2062.2	Ap ^r Gm ^r	<i>tuf</i>	<i>eyfp</i>	++	++	–
pTK165-D	pISM2062.2	Ap ^r Gm ^r Cm ^r	<i>tuf</i>	<i>eyfp</i>	NT	NT	NT
pTK205	pKV104	Ap ^r Cm ^r	<i>lac (E. coli)</i>	<i>ecfp</i>	NT	NT	NT
pTK207	pKV104	Ap ^r Cm ^r	<i>tuf</i>	<i>ecfp</i>	++	++	–
pTK207-D	pKV104	Ap ^r Cm ^r	<i>tuf</i>	<i>ecfp</i>	NT	NT	NT
pTK210	pTK207-D	Ap ^r Cm ^r	<i>tuf</i>	<i>ecfp-p65</i>	++	++	+
pMPN310-E	pENTR/D-TOPO	Km ^r	None	<i>hmw2</i>	NT	NT	NT
pMPN311-E	pDONR201	Km ^r	None	<i>p41</i>	NT	NT	NT
pMPN312-E	pDONR201	Km ^r	None	<i>p24</i>	NT	NT	NT
pMPN310	pTK164-D	Ap ^r Gm ^r	<i>p65</i>	<i>eyfp-hmw2</i>	+	+	+
pMPN311	pTK164-D	Ap ^r Gm ^r	<i>p65</i>	<i>eyfp-p41</i>	+	+	+
pMPN312	pTK164-D	Ap ^r Gm ^r	<i>p65</i>	<i>eyfp-p24</i>	+	+	+
pMPN310-tuf	pTK165-D	Ap ^r Gm ^r	<i>tuf</i>	<i>eyfp-hmw2</i>	++	++	+
pMPN311-tuf	pTK165-D	Ap ^r Gm ^r	<i>tuf</i>	<i>eyfp-p41</i>	++	++	+
pMPN312-tuf	pTK165-D	Ap ^r Gm ^r	<i>tuf</i>	<i>eyfp-p24</i>	++	++	+

^a *M. pneumoniae* strains transformed with Tn4001 plasmids were analyzed by Western blotting and fluorescence microscopy. NT, not applicable or not tested.

^b Expression of the fusion protein in *M. pneumoniae* cells was monitored by Western blotting: +, ++, and –, moderate, strong, and no expression, respectively.

^c Fluorescence intensity was observed by microscopy: +, ++, and –, faint, strong, and no fluorescence, respectively.

^d Localization of the fusion protein at cell poles was observed by microscopy: +, present; –, absent.

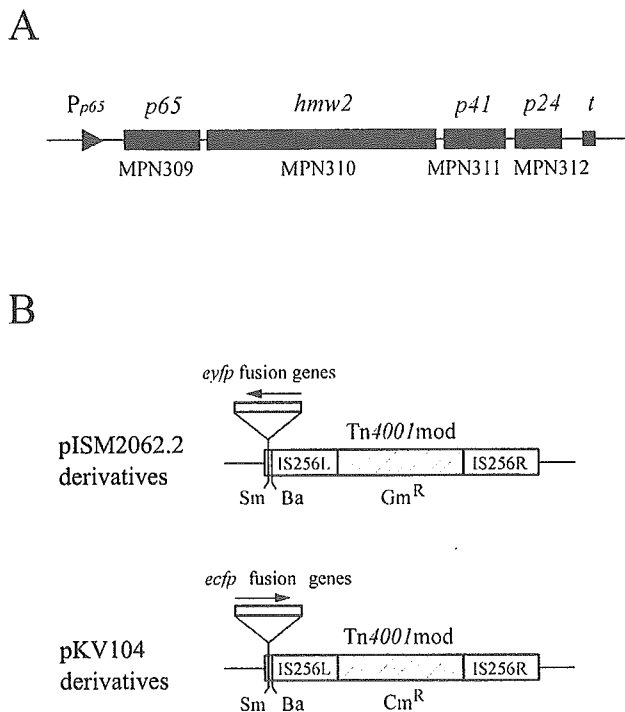


FIG. 1. (A) Schematic illustration of the *crl* operon of *M. pneumoniae*. The four rectangular bars indicate the *p65*, *hmw2*, *p41*, and *p24* genes in this operon. These genes are also designated MPN309, MPN310, MPN311, and MPN312 according to the serial numbering system of the *M. pneumoniae* genome project (8). The triangle and the square represent the *p65* promoter (P_{p65}) and the terminator (t) of this operon, respectively. The figure is not drawn precisely to scale. (B) Structures of modified staphylococcal transposon Tn4001mod vectors (11, 22). Plasmid pISM2062.2 carries a Gm^r version of Tn4001mod. Plasmid pKV104 carries a Cm^r version of Tn4001mod. The IS256L, IS256R, and drug resistance genes (Gm^r and Cm^r) of Tn4001mod are illustrated. Cloning sites (Sm, SmaI; Ba, BamHI) in Tn4001mod are indicated. The *eyfp* fusion genes were inserted into the SmaI site of pISM2062.2. The *ecfp* fusion genes were inserted into the SmaI site of pKV104. The arrows indicate the directions in which the fusion genes were inserted.

with a 0.45- μ m-pore size (Millipore, Billerica, Mass.) to disperse aggregates (46, 48), and placed on coverslips cleaned with saturated ethanolic KOH (4). The coverslips with the cell suspensions were incubated at 37°C for 0.5 to 1 h and were mounted on glass slides after excess cell suspensions were removed. To observe ECFP fluorescence, coverslips were washed twice with phosphate-buffered saline before being mounted on glass slides to reduce background fluorescence. The cells were observed with a BX51 fluorescence microscope equipped with YFP and CFP filter units (U-MYFPHQ and U-MCFPHQ, respectively) and a phase-contrast setup (Olympus, Tokyo, Japan). The images were digitized by using a Photometrics CoolSNAPcf charge-coupled device camera (Roper Scientific, Atlanta, Ga.) and LuminaVision software (Mitani Corp., Tokyo, Japan); signals were adjusted to obtain proper intensities. The fluorescence images were pseudocolored by using the LuminaVision software. The images were also processed by using Adobe Photoshop software, versions 6.0 and 7.0 (Adobe Systems, San Jose, Calif.).

To observe gliding, cells of strain TK162 were suspended in saline containing 20% horse serum. The cell suspension was inserted into a tunnel that was 12 mm wide, 18 mm long, and 0.06 mm high and that was assembled from a glass slide, a coverslip, and two pieces of double-sided tape; the cells were incubated in this tunnel for 10 min at 37°C. The cells then were observed with the fluorescence microscope at 37°C; this temperature was achieved by attaching a heating system to the sample stage and the objective lens. Cell images were recorded by using a charge-coupled device camera (WV-BP510; Panasonic, Osaka, Japan) and a digital videocassette recorder (WV-D9000; Sony, Tokyo, Japan) and were digitized as described previously (37).

RESULTS

Construction of the *p65* fusion genes and their expression in *M. pneumoniae* cells. We chose the P65 protein as the initial target for the fluorescent-protein tagging strategy by virtue of the location of its gene just downstream of the promoter of the *crl* operon (28) (Fig. 1A); this promoter can be used to express recombinant *p65* genes. The *eyfp* gene, encoding EYFP, which is a yellow-green-shifted variant of GFP that gives a stronger fluorescence emission than the wild type (10), was fused to the 3' or 5' end of the *p65* gene. The fusion genes were under the control of the native *p65* promoter and were inserted into the SmaI site of Tn4001mod vector plasmid pISM2062.2 (22) (Fig. 1B). The plasmids that we designated pTK155 and pTK161 carry the *p65-eyfp* and *eyfp-p65* fusion genes, respectively (Table 3). These plasmids were introduced into *M. pneumoniae* M129 by electroporation to deliver fusion genes to the chromosome by the transposition of Tn4001mod. Transformants TK155 and TK161 (named for plasmids pTK155 and pTK161, respectively) were obtained and were examined by fluorescence microscopy, which detected faint fluorescent signals from both strains. In most cells, the signals were located at one pole (Fig. 2), suggesting that the P65-EYFP and EYFP-P65 fusions were produced in these strains and localized at the attachment organelle. The intensities of the fluorescence signals were similar between the strains but slightly stronger in TK161 (Fig. 2).

To enhance the fluorescence intensity, we chose the *eyfp-p65* fusion gene, which exhibited slightly brighter fluorescence, and

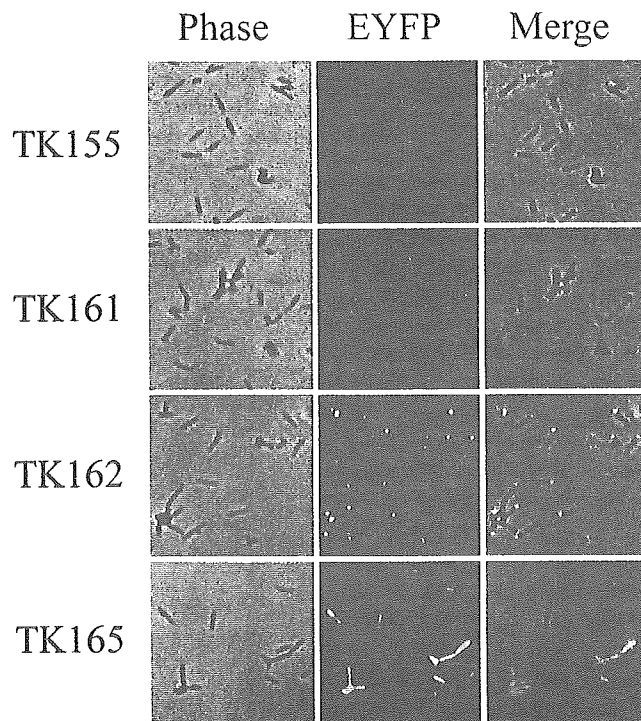


FIG. 2. Subcellular localization of EYFP fusions. The left and middle panels in each row show the same cells observed by phase-contrast microscopy and fluorescence microscopy, respectively. The right panel in each row shows the merged image of the left and middle panels. The transformants are named at left. Bar, 5 μ m.

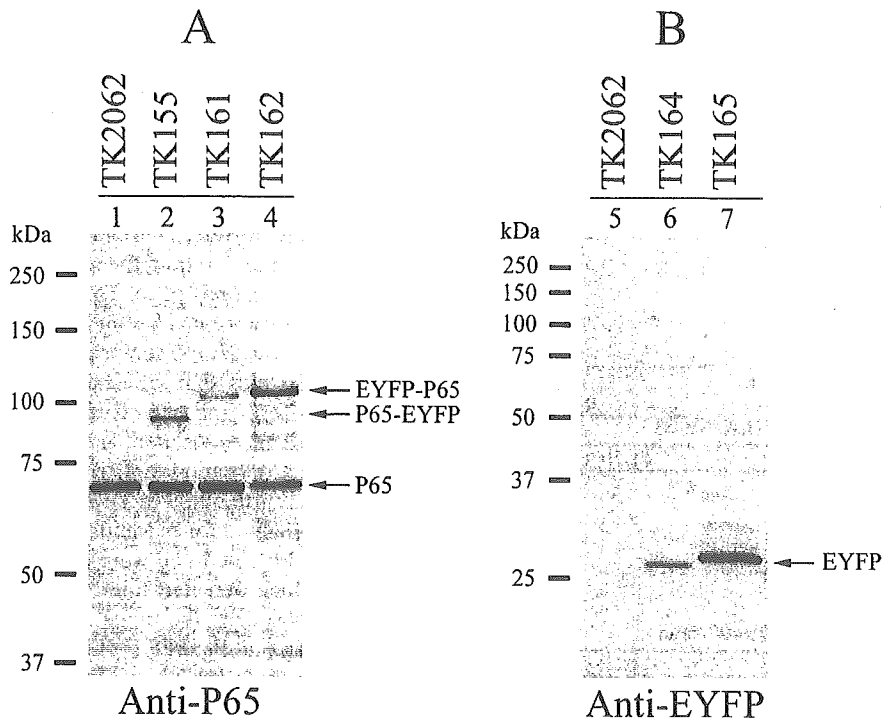


FIG. 3. Expression of fusions of P65 and EYFP in *M. pneumoniae* cells. (A) Western blot analysis of *M. pneumoniae* transformants with an anti-P65 antibody. Lysates of *M. pneumoniae* transformant cells (5 μ g of total protein) were separated by SDS-8% PAGE, transferred to a nitrocellulose membrane, and probed with an anti-P65 antibody. The positions of the detected P65-EYFP, EYFP-P65, and native P65 are indicated by arrows. Molecular sizes are shown at left. The analyzed transformants are shown above the lanes. (B) Detection of EYFP expression by Western blot analysis. Lysates of *M. pneumoniae* transformant cells (5 μ g of total protein) were separated by SDS-12% PAGE. The position of EYFP detected by an anti-EYFP (anti-GFP variant) antibody is indicated by an arrow. Molecular sizes are shown at left. The analyzed transformants are shown above the lanes.

we tested a promoter sequence of the *tuf* gene of *M. pneumoniae* instead of the *p65* promoter. Plasmid pTK162, which carries the *eyfp-p65* fusion gene under the control of the *tuf* promoter, was constructed and used to transform *M. pneumoniae* M129. The strain obtained, TK162, showed strong fluorescent signals at the cell poles (Fig. 2), suggesting higher production of the EYFP-P65 fusion in TK162 than in TK161. To confirm whether the polar localization of fusion proteins depends on the P65 moiety, we constructed plasmids pTK164 and pTK165, which carried the *eyfp* gene alone under the control of the *p65* or the *tuf* promoter (Table 3). The transformants with these plasmids, TK164 and TK165, showed fluorescence throughout the whole cell body (Fig. 2; only TK165 is shown), indicating that the polar localization of the P65-EYFP and EYFP-P65 fusions is caused by the properties of the P65 moiety. The intensity of EYFP fluorescence was strong in TK165 but faint in TK164, corresponding to their promoter activities.

We next analyzed transformant strains by Western blot analysis to examine the levels of expression of fusion proteins. By using anti-P65 antiserum, we detected P65-EYFP in TK155 and EYFP-P65 in both TK161 and TK162 (Fig. 3). TK155 and TK161 both had lower levels of fusion proteins than of native P65 (Fig. 3, lanes 2 and 3). On the other hand, the level of expression of EYFP-P65 in TK162 was comparable to that of native P65 (Fig. 3, lane 4). The size difference between P65-EYFP and EYFP-P65 (Fig. 3, lanes 2, 3, and 4) was caused by the addition of a short amino acid sequence at the N terminus

of EYFP-P65, which resulted from the construction of the promoter fusion. The anti-EYFP antibody detected EYFP in both TK164 and TK165 (Fig. 3, lanes 6 and 7). The level of EYFP was low in TK164 but high in TK165, reflecting the activities of the *p65* and *tuf* promoters. The size difference for EYFP between TK164 and TK165 was attributed to the construction of the promoter fusion. These results indicated that the fluorescence intensities of the transformants correlated with their levels of EYFP fusion expression.

The fluorescence diminished in 10 s even in TK165 cells, with the highest intensity. This rather rapid bleaching may be attributable to the small number of fluorescent molecules caused by the small dimensions of *M. pneumoniae* cells. An *M. pneumoniae* cell is about 2 μ m in length and 0.2 μ m in diameter. The total volume is estimated to be 25 times lower than that of an *E. coli* cell. The signal from the small number of fluorescent molecules may easily fall below the detection limit as a result of photobleaching of the molecules.

The cytoadherence ability of the transformants was also analyzed by a standard hemadsorption (HA) assay (14, 27). Of the colonies tested, 97% showed HA activity, suggesting that the expression of the EYFP fusions did not disturb the cytoadherence processes of *M. pneumoniae*. However, 3% of the colonies did not show HA activity. This frequency of HA-negative colonies, obviously higher than that caused by spontaneous mutation (27), may have been caused by the insertion of Tn4001 into the cytoadherence-related genes.

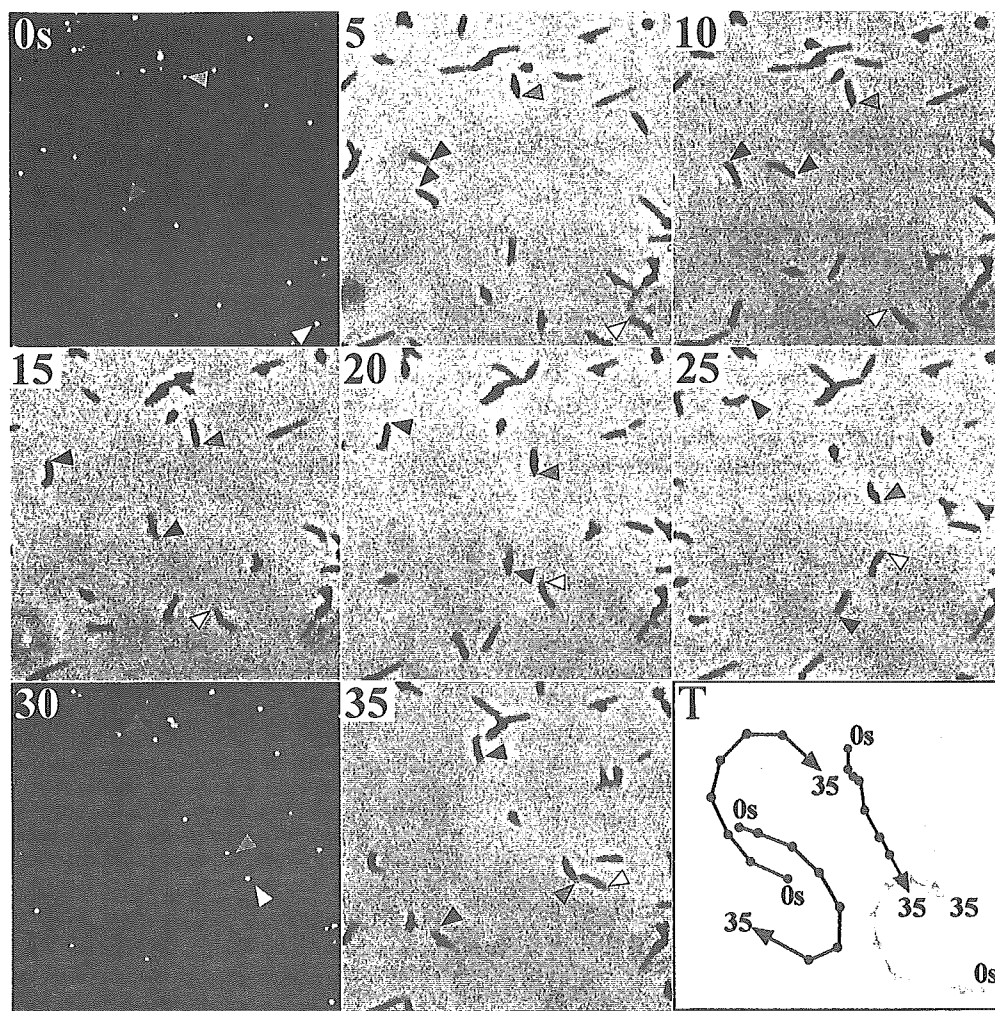


FIG. 4. Gliding motility of *M. pneumoniae* cells whose attachment organelles are fluorescently labeled with the EYFP-P65 fusion. Strain TK162 was observed by phase-contrast microscopy and fluorescence microscopy at 37°C. The phase-contrast image was recorded continuously with a video recorder. The microscope was shifted to the fluorescence setup for 2 s at 28-s intervals. The time intervals between images in this figure are 5 s. The positions of attachment organelles of four typical cells are indicated by colored arrowheads. The tracks of cell movement (positions of attachment organelles) are shown by colored lines in the bottom right panel (T). Bar, 5 μ m.

Observation of gliding cells. Bretz (6, 7) and Radestock and Bretz (42) studied the gliding motility of *M. pneumoniae* cells by phase-contrast microscopy and concluded that the attachment organelle functions as the leading end of gliding cells. If EYFP-P65 fusions are properly incorporated into the attachment organelle, then the fluorescent foci must be observed at the leading end of gliding *M. pneumoniae* cells. To confirm this notion directly, we studied the gliding motility of TK162 cells, which exhibited the brightest fluorescent foci among the TK strains. To do so, we made slight modifications to a method used to observe the gliding of *Mycoplasma mobile* cells (35). TK162 cells were suspended in saline including 20% horse serum and were inserted into a tunnel assembled from a glass slide and a coverslip. We excluded heart infusion broth and yeast extract from the cell suspension, because these components of mycoplasma growth medium cause strong background fluorescence. The coverslip was maintained at 37°C on the microscope stage. Gliding cells on the glass surface and fluorescent foci were observed by phase-contrast microscopy and

fluorescence microscopy, respectively (Fig. 4). As expected, the fluorescent focus was always positioned ahead of the gliding cell, indicating the localization of EYFP-P65 at the attachment organelle. In gliding cells, the attachment organelle (fluorescent focus) always moved smoothly, while the other part of the cell body often showed lateral wobble motion, consistent with previous observations (6, 7, 42). These results suggested that the organelle kept contact with the glass surface and that the other part of the cell body detached from the surface during gliding.

The proportion of gliding cells was apparently higher in saline containing 20% serum than in growth medium (unpublished data). Nutrient-starved conditions may accelerate the movement, as observed in other gliding bacteria (32). The addition of 1 to 5% gelatin was not needed with our conditions, although it has been reported to be essential for keeping cells on the glass surface (42). This difference may be related to differences in glass surface conditions between previous studies and our investigation.

The average speed of the gliding shown in Fig. 4 was calculated to be 0.40 $\mu\text{m/s}$, consistent with previous observations (6, 21, 42). We tried multiple times to observe the cell division process of *M. pneumoniae* during 30 min of continuous video recording but failed to find cells that exhibited nascent attachment organelle formation or cytokinesis.

Subcellular localization of the HMW2, P41, and P24 proteins. We extended the fluorescent-protein tagging strategy to the other gene products of the *crl* operon (the HMW2, P41, and P24 proteins) (Fig. 1A). Although the polar localization of HMW2 at the attachment organelle was reported recently by Balish et al. (3), the localization of P41 and P24 was unknown. For these experiments, we introduced a second fluorescent protein, ECFP (a blue-colored derivative of GFP) (10), to mark the positions of the attachment organelles of living cells. The *ecfp* gene was fused to the 5' end of the *p65* gene and was under the control of the *tuf* promoter. This *ecfp-p65* fusion gene was introduced into *M. pneumoniae* M129 by use of a Cm^r derivative of Tn4001mod (11) (Fig. 1B). The resulting Cm^r transformant, which we designated TK210, expressed ECFP-P65 at a level slightly lower than that of native P65 (Fig. 5A) and exhibited blue fluorescent signals at the cell poles (attachment organelle) (Fig. 5B). We used TK210 as a host strain to examine the subcellular localization of HMW2, P41, and P24.

We constructed two groups of plasmids for the expression of EYFP fusions of HMW2, P41, and P24 by modifying plasmids pTK164 and pTK165 (Table 3). The first group of plasmids was designated pMPN (derivatives of pTK164); each of these plasmids possessed the *eyfp-hmw2*, *eyfp-p41*, or *eyfp-p24* fusion genes under the control of the *p65* promoter for low-level expression (Table 3). The second group of plasmids, designated pMPN-*tuf* (derivatives of pTK165) (Table 3), contained the *eyfp-hmw2*, *eyfp-p41*, or *eyfp-p24* fusion genes under the control of the *tuf* promoter for high-level expression. These plasmids were introduced into strain TK210, and Cm^r - Gm^r transformants were obtained. Western blot analysis for the fusion proteins confirmed that transformants TK2310, TK2311, and TK2312 (created with pMPN plasmids) expressed EYFP-HMW2, EYFP-P41, and EYFP-P24 at low levels (Fig. 6A), while transformants TK2310T, TK2311T, and TK2312T (created with pMPN-*tuf* plasmids) expressed them at higher levels (Fig. 6B). The EYFP fluorescent signals of strains with low-level expression were weak and were captured with an exposure time longer than that of strains with high-level expression (Fig. 7).

Strains TK2310 and TK2310T expressing EYFP-HMW2 showed fluorescent signals for EYFP at their cell poles. The distribution patterns for fluorescent foci were basically identical between the two strains, regardless of the level of expression of EYFP-HMW2, but the fluorescence signal intensities reflected the expression levels, as indicated by the difference in brightness between the focus signals and the background of the EYFP images (Fig. 7). In both strains, the fluorescent foci of EYFP-HMW2 almost overlapped those of ECFP-P65 (Fig. 7), indicating that the HMW2 protein was localized at the attachment organelle. These results confirmed the findings of Balish et al. (3).

Transformants TK2311, TK2312, TK2311T, and TK2312T revealed that EYFP-P41 and EYFP-P24 formed fluorescent foci in *M. pneumoniae* cells (Fig. 7). Unlike EYFP-HMW2, the

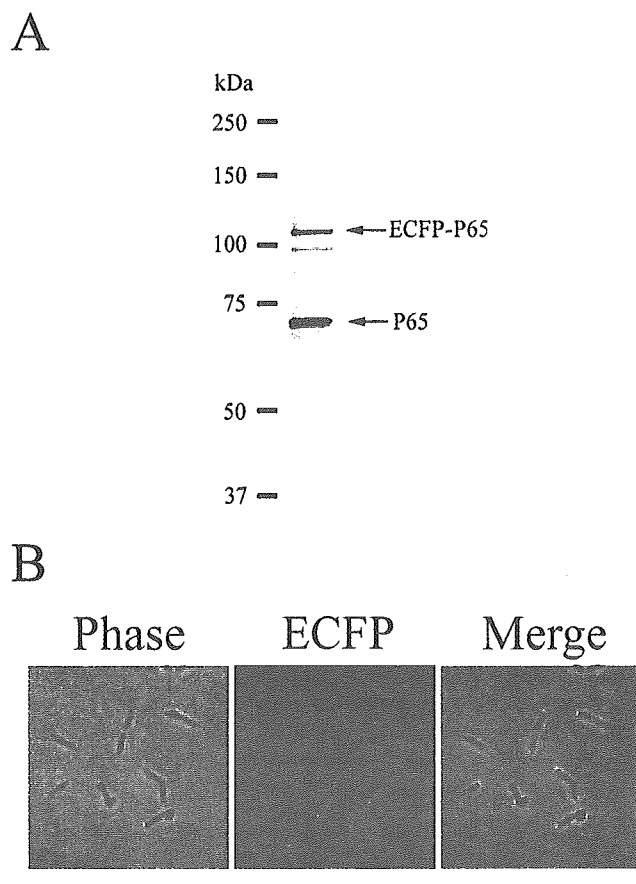


FIG. 5. Western blot analysis and fluorescence microscopy of *M. pneumoniae* TK210. (A) Western blot analysis of *M. pneumoniae* strain TK210. Lysates of *M. pneumoniae* TK210 cells (5 μg of total protein) were separated by SDS-8% PAGE, transferred to a nitrocellulose membrane, and probed with an anti-P65 antibody. The positions of the detected ECFP-P65 and native P65 are indicated by arrows. Molecular sizes are shown at left. (B) Subcellular localization of the ECFP-P65 fusion. The left and middle panels show the same cells observed by phase-contrast microscopy and fluorescence microscopy, respectively. The right panel shows the merged image of the left and middle panels. Bar, 5 μm .

foci of EYFP-P41 and EYFP-P24 were located mainly at the proximal region of the attachment organelle and did not overlap those of ECFP-P65. In strains showing low-level expression of EYFP-P41 or EYFP-P24 (TK2311 and TK2312), the fluorescent foci of these proteins were confined to the proximal end of the attachment organelle (Fig. 7), and the profiles of these proteins were very similar. However, in strains showing high-level expression (TK2311T and TK2312T), the distribution patterns for fluorescent signals were not identical between EYFP-P41 and EYFP-P24 (Fig. 7). In strain TK2311T, additional fluorescent foci for EYFP-P41 were frequently observed at the opposite end of the attachment organelle, i.e., at the cell tail (Fig. 7). On the other hand, the fluorescence signals for EYFP-P24 were diffused from the proximal end of the organelle to the cell tail (Fig. 7, TK2312T). These nonidentical distribution patterns for EYFP-P41 and EYFP-P24 in strains showing high-level expression suggested that these proteins had different properties in the cells. However, even in these strains showing high-level expression, the strongest signals

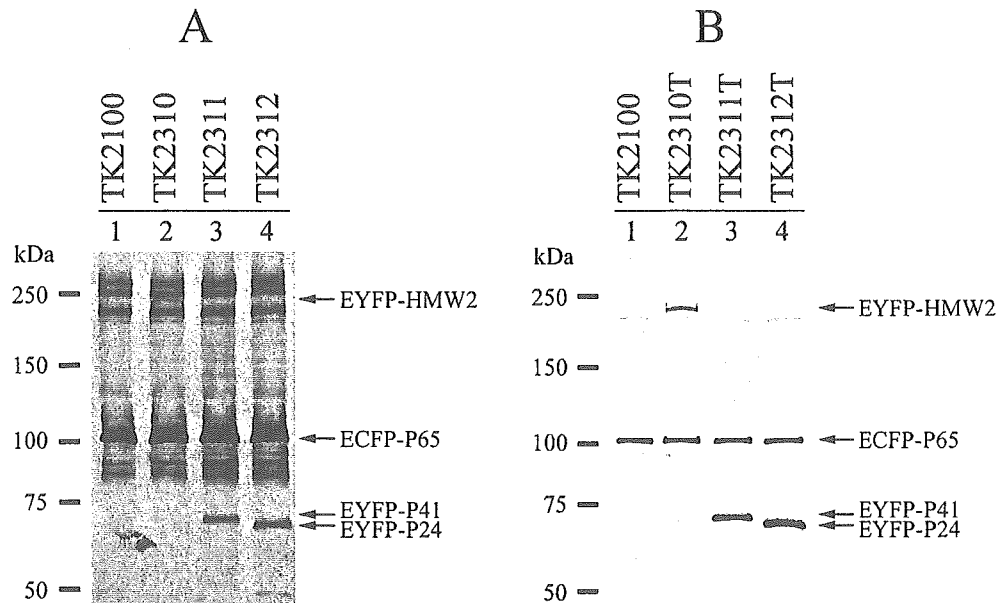


FIG. 6. Expression of EYFP-HMW2, EYFP-P41, and EYFP-P24 fusions in *M. pneumoniae* cells. (A) Western blot analysis of low-level expression transformants of EYFP fusions. Lysates of *M. pneumoniae* transformant cells (TK2100, TK2310, TK2311, and TK2312) (10 μ g of total protein) were separated by SDS-5 to 10% gradient PAGE, transferred to a nitrocellulose membrane, and probed with an anti-GFP variant antibody. The positions of detected EYFP-HMW2, EYFP-P41, EYFP-P24, and ECFP-P65 are indicated by arrows. Molecular sizes are shown at left. (B) Western blot analysis of high-level expression transformants. Lysates of *M. pneumoniae* transformant cells (TK2100, TK2310T, TK2311T, and TK2312T) (5 μ g of total protein) were analyzed under the same conditions in those used in panel A. The positions of detected fusion proteins are indicated by arrows.

were located at the proximal end of the organelle, suggesting that this site is the preferential localization site for both P41 and P24.

We also transformed *M. pneumoniae* M129 with the pMPN and pMPN-tuf plasmids, and the *eyfp-hmw2*, *eyfp-p41*, and *eyfp-p24* fusion genes were expressed (strains TK3310, TK3311, TK3312, TK3310T, TK3311T, and TK3312T). We confirmed that the localization patterns for EYFP-HMW2, EYFP-P41, and EYFP-P24 in the background of strain M129 were identical to those in the background of strain TK210 (Fig. 8A; only the images for TK3310T, TK3311T, and TK3312T are shown); these results indicate that the presence of ECFP-P65 does not affect the localization of these EYFP fusions.

DISCUSSION

Fluorescent-protein tagging is a widely used strategy for visualizing proteins in living cells. In this study, we have constructed vectors for fluorescent-protein tagging in *M. pneumoniae* and used them to visualize the protein components of cytoskeleton-like structures. The vectors constructed in this study are based on the Tn4001mod vector system (11, 22) and possess *M. pneumoniae* *p65* or *tuf* promoters for the expression of fluorescent target proteins. These two promoters allow for high and low levels of expression of target proteins and are helpful for enhancing the resolution of fluorescent images and assessing the patterns of localization of target proteins. We used EYFP and ECFP as fluorescent-protein tags and designed a coexpression procedure for these proteins. This procedure enabled dual labeling of two target proteins in living *M. pneumoniae* cells. Since *M. pneumoniae* cells are pleomorphic,

it is sometimes difficult to judge the position of the attachment organelle in the cell. The dual-labeling method made it easier to ascertain the position of the organelle relative to the target protein. The first fluorescent protein can be used to label the organelle, while the second is used for the other target proteins.

Using our fluorescent-protein tagging method, we visualized the four proteins—P65, HMW2, P41, and P24—that are encoded in the *crl* operon (Fig. 1A). The P65 protein labeled with EYFP was localized at the attachment organelle (Fig. 2), confirming previous observations obtained by immunofluorescence microscopy (20, 48, 49). The localization of P65 at the organelle indicates that P65 is a component of the attachment organelle. However, neither the function of P65 nor its involvement in cytoadherence is fully understood, mainly because of the lack of P65 mutant strains. It is known that P65 is present at reduced steady-state levels in mutant strains that lack any of the cytoadherence accessory proteins—HMW1, HMW2, HMW3, and P30. In these mutant strains, the polar localization of P65 is partially disrupted, depending on the extent to which the P65 levels are reduced (2, 20, 52). The stability and polar localization of P65 are thought to be correlated. To stabilize P65, it may be necessary to incorporate it into the stable localization site at the organelle. This stable localization site may be provided by the other cytoskeletal proteins (25). Unincorporated P65 tends to be degraded by proteolysis. Consistent with this model, in strain TK162, expressing a high level of EYFP-P65, the level of native P65 was lower than the levels in the other strains (Fig. 3, lane 4). It is likely that the localization site for P65 at the organelle was occupied by an excess of EYFP-P65 in this strain and that unincorporated native P65 and EYFP-P65 were degraded. This sce-

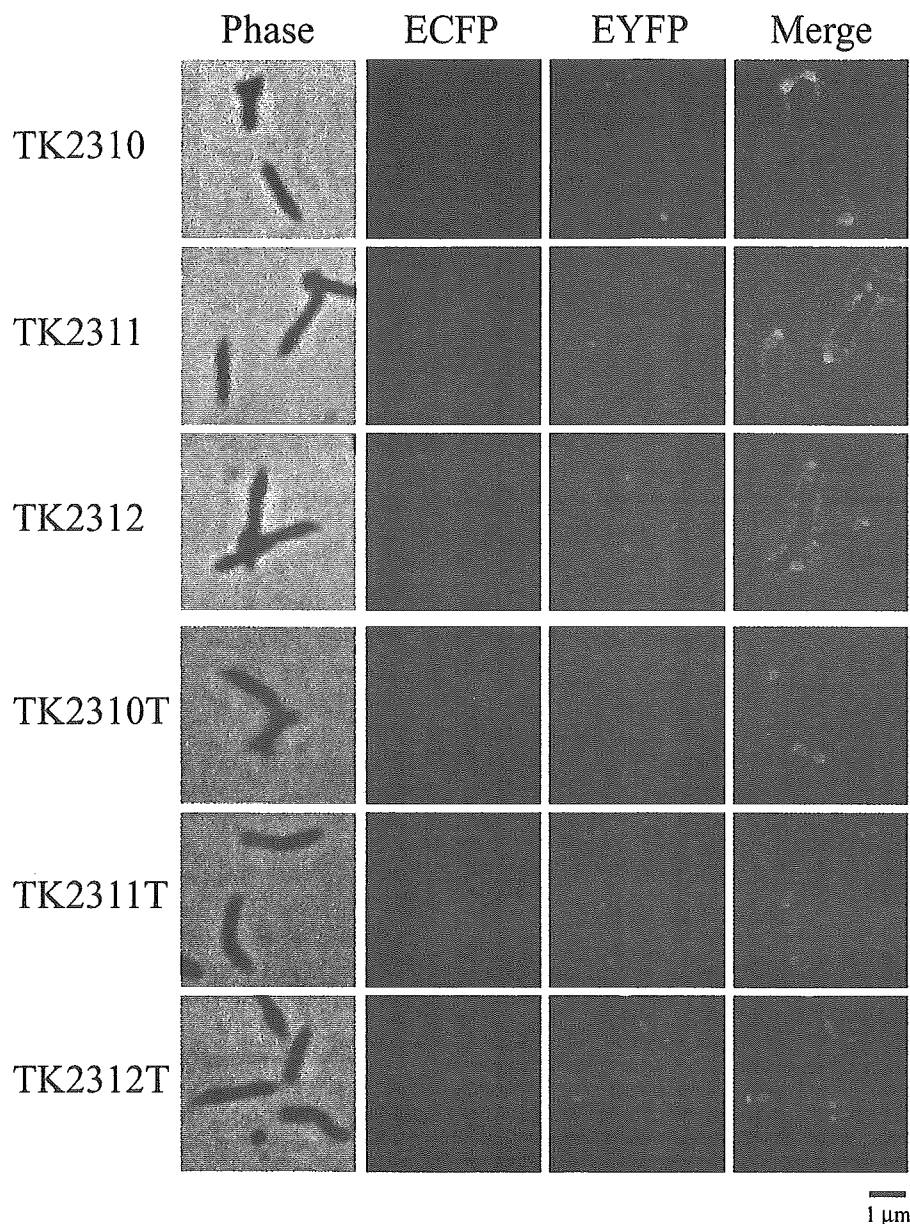


FIG. 7. Subcellular localization of EYFP-HMW2, EYFP-P41, and EYFP-P24 fusions in the *M. pneumoniae* TK210 cell background. Images of six *M. pneumoniae* transformants (names at left) are shown. The first panel in each row shows the phase-contrast image of the cells. The second and third panels in each row show ECFP and EYFP fluorescence images of the same cells, respectively. The fourth panel in each row shows the merged image of the phase-contrast and fluorescence images. Transformants TK2310, TK2311, and TK2312 show low levels of expression of EYFP-HMW2, EYFP-P41, and EYFP-P24, respectively; transformants TK2310T, TK2311T, and TK2312T show high levels of expression. Bar, 1 μ m.

nario may also explain the clear focal fluorescence signals of EYFP-P65 at the attachment organelle and the lesser amounts of additional fluorescence in other parts of *M. pneumoniae* cells, even with high-level expression of EYFP-P65 (Fig. 2). Because EYFP-P65 gave clear focal fluorescence signals at the organelle, we also labeled P65 with ECFP and used ECFP-P65 as a positional marker of the organelle for examining the localizations of the other proteins (Fig. 5).

The HMW2 protein is a critical factor for cytoadherence. It is thought to function in the early stage of assembly of the attachment organelle, together with the HMW1 protein (25). The loss of HMW2 affects the stability and polar localization of

most of the other cytoadherence accessory proteins, but HMW2 itself is also less stable in the absence of HMW1 (2). The EYFP-HMW2 fusion was localized at the attachment organelle when expressed at both high and low levels (Fig. 7), supporting the observations of Balish et al. (3). The localization sites for EYFP-HMW2 were almost identical to those for ECFP-P65 coexpressed in the same cells. However, in a considerable number of these cells, the fluorescence signals from EYFP-HMW2 extended slightly farther toward the proximal end than did the signals from ECFP-P65, which were relatively limited to the distal end of the organelle (data not shown). These observations agree with previous ones (49) and with the cur-

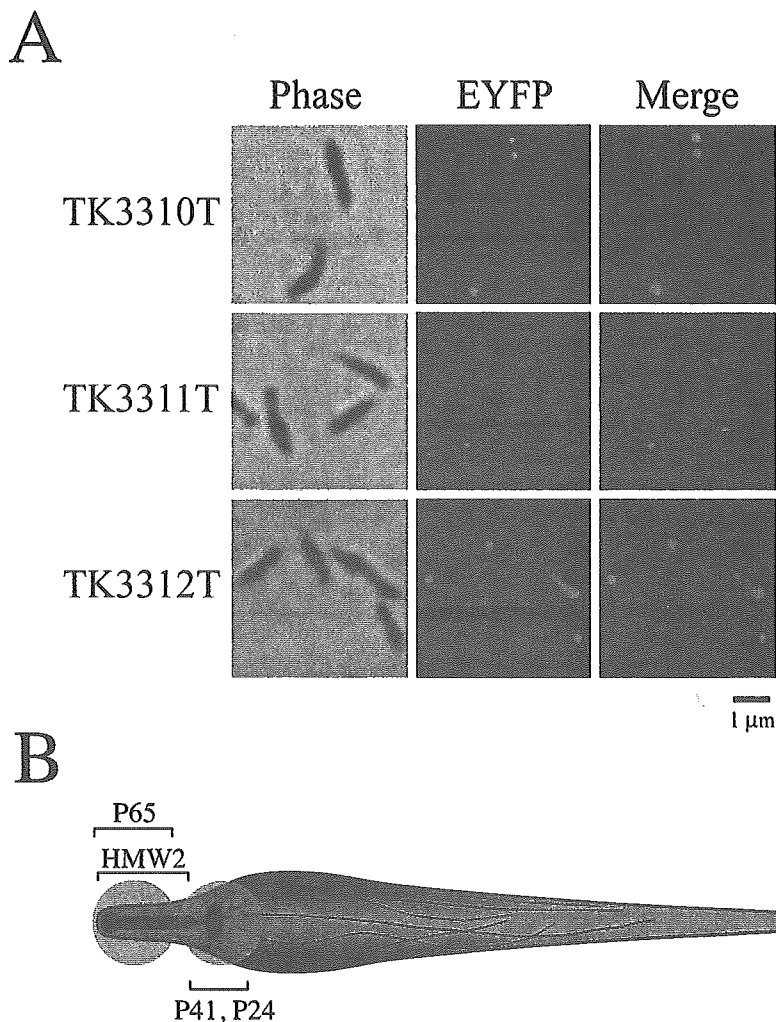


FIG. 8. (A) Subcellular localization of EYFP-HMW2, EYFP-P41, and EYFP-P24 fusions in the wild-type *M. pneumoniae* M129 cell background (without ECFP-P65). The left and middle panels in each row show images of the same cells observed by phase-contrast microscopy and fluorescence microscopy, respectively. The right panel in each row shows the merged image of the left and middle panels. The transformants are named at left. Bar, 1 μ m. (B) Schematic illustration of an *M. pneumoniae* cell. Cytoskeleton-like structures within the *M. pneumoniae* cell (electron-dense core, wheel-like structure, and fibrous network) are illustrated (see the text). Approximate positions of the fluorescent signals observed by microscopy are shown with colors (blue, ECFP-P65; green, EYFP-P41 and EYFP-P24). Positions of sites of localization of P65, HMW2, P41, and P24 are indicated.

rent structural model of the organelle, which proposes that P65 is localized at the surface of the distal end of the attachment organelle and that HMW2 is the most probable component of the electron-dense core (25).

Little is known about the P41 and P24 proteins (25, 28). A homologous gene for P41 is present in the closely related species *Mycoplasma genitalium* (17), but no homologous gene has been found for P24. Although the functions of P41 and P24 are unknown, both attract considerable interest as cytoskeletal proteins, since they are encoded in the *crI* operon, together with P65 and HMW2, and are associated with the Triton shell (H. Ogaki et al., unpublished data). In addition, the P41 protein is predicted to contain a coiled-coil structure that has been observed in the other cytoskeletal proteins. Therefore, we analyzed the subcellular localization of these proteins by fluorescent-protein tagging and demonstrated that EYFP-P41 and EYFP-P24 were preferentially localized at the proximal end of

the attachment organelle in *M. pneumoniae* cells, suggesting that they are cytoskeletal proteins that form unknown structures at this site. However, it should be noted that the high-level expression of both of these proteins exhibited additional fluorescent signals in the cells (Fig. 7). We thought that these additional localization patterns were caused by accumulations of excess proteins in the cells, but it remains possible that these localization patterns in cells with high-level expression reflect the native localization patterns for P41 and P24. This point must be assessed by using another method, such as immunofluorescence. If P41 and P24 really do localize to the proximal end of the attachment organelle, then what structures are present at this site? Recently, the presence of a wheel-like complex that might be part of a cytoskeleton-like structure was suggested at the proximal end of the electron-dense core by transmission electron microscopy of an ultrathin section of *M. pneumoniae* cells (16). This wheel-like complex is structurally

similar to the flagellar motor and might be connected to fibrous structures extending into the cytoplasm of *M. pneumoniae* cells. The detailed structure of this wheel-like complex has yet to be elucidated, but its position (at the proximal end of the electron-dense core) corresponds to the P41 and P24 localization site (Fig. 8B).

We also used the fluorescent-protein tagging technique to observe gliding *M. pneumoniae* cells (Fig. 4). The expression of EYFP-P65 in *M. pneumoniae* allowed real-time visualization of the attachment organelle of gliding cells by phase-contrast and fluorescence microscopy. The successful labeling of the attachment organelle of living *M. pneumoniae* cells indicated that this technique should be applicable to the direct observation of the cell division processes in *M. pneumoniae* (i.e., nascent organelle formation, the migration of one of the organelles to the opposite end, and cytokinesis) (34, 36, 48). However, an attempt at such an application was not successful in this study. The major reason for this result might have been the nutrient conditions of *M. pneumoniae* cells used for microscopy. We used saline containing 20% horse serum to suspend cells for fluorescence microscopy in order to reduce background fluorescence. Such low-nutrient conditions might not be sufficient to support cell division in *M. pneumoniae*. If cell division did somehow occur under these conditions, then a longer observation time might have been required, since the doubling time of *M. pneumoniae* M129 is estimated to be about 10 h, even under optimal conditions (31). In future studies, these situations could be improved by reducing the background fluorescence in the medium or by using fusion proteins with more intense signals.

ACKNOWLEDGMENTS

We are grateful to D. C. Krause of the University of Georgia for providing plasmid pKV104 and to C. Citti of the University of Veterinary Medicine, Vienna, Austria, for providing plasmid pISM2062.2. We thank Y. Arakawa of the National Institute of Infectious Diseases, Tokyo, Japan, for helpful input.

This work was supported in part by a Grant-in-Aid for JSPS Fellows from the Japan Society for the Promotion of Science (to S.S.) and by Grants-in-Aid for Young Scientists (to A.H.), for Scientific Research (to M.M.), and for Science Research on Priority Areas (motor proteins, genome science, and infection and host response) (to M.M.) from the Ministry of Education, Culture, Sports, Science, and Technology of Japan.

REFERENCES

- Aluotto, B. B., R. G. Wittler, C. O. Williams, and J. E. Faber. 1970. Standardized bacteriologic techniques for the characterization of mycoplasma species. *Int. J. Syst. Bacteriol.* **20**:35–58.
- Balish, M. F., and D. C. Krause. 2002. Cytadherence and cytoskeleton, p. 491–518. *In* S. Razin and R. Herrmann (ed.), *Molecular biology and pathogenicity of mycoplasmas*. Kluwer Academic/Plenum Publishers, New York, N.Y.
- Balish, M. F., R. T. Santurri, A. M. Ricci, K. K. Lee, and D. C. Krause. 2003. Localization of *Mycoplasma pneumoniae* cytodherence-associated protein HMW2 by fusion with green fluorescent protein: implications for attachment organelle structure. *Mol. Microbiol.* **47**:49–60.
- Berg, H. C., and L. Turner. 1993. Torque generated by the flagellar motor of *Escherichia coli*. *Biophys. J.* **65**:2201–2216.
- Biberfeld, G., and P. Biberfeld. 1970. Ultrastructural features of *Mycoplasma pneumoniae*. *J. Bacteriol.* **102**:855–861.
- Bredt, W. 1968. Motility and multiplication of *Mycoplasma pneumoniae*. A phase contrast study. *Pathol. Microbiol. (Basel)* **32**:321–326.
- Bredt, W. 1973. Motility of mycoplasmas. *Ann. N. Y. Acad. Sci.* **225**:246–250.
- Dandekar, T., M. Huynen, J. T. Regula, B. Ueberle, C. U. Zimmermann, M. A. Andrade, T. Doerks, L. Sanchez-Pulido, B. Snel, M. Suyama, Y. P. Yuan, R. Herrmann, and P. Bork. 2000. Re-annotating the *Mycoplasma pneumoniae* genome sequence: adding value, function and reading frames. *Nucleic Acids Res.* **28**:3278–3288.
- Feldner, J., U. Gobel, and W. Bredt. 1982. *Mycoplasma pneumoniae* adhesin localized to tip structure by monoclonal antibody. *Nature* **298**:765–767.
- Green, G., S. R. Kain, and B. Angres. 2000. Dual color detection of cyan and yellow derivatives of green fluorescent protein using conventional fluorescence microscopy and 35-mm photography. *Methods Enzymol.* **327**:89–94.
- Hahn, T. W., E. A. Mothershed, R. H. Waldo, and D. C. Krause. 1999. Construction and analysis of a modified Tn4001 conferring chloramphenicol resistance in *Mycoplasma pneumoniae*. *Plasmid* **41**:120–124.
- Hahn, T. W., M. J. Willby, and D. C. Krause. 1998. HMW1 is required for cytodhesin P1 trafficking to the attachment organelle in *Mycoplasma pneumoniae*. *J. Bacteriol.* **180**:1270–1276.
- Hanahan, D. 1983. Studies on transformation of *Escherichia coli* with plasmids. *J. Mol. Biol.* **166**:557–580.
- Hansen, E. J., R. M. Wilson, and J. B. Baseman. 1979. Isolation of mutants of *Mycoplasma pneumoniae* defective in hemadsorption. *Infect. Immun.* **23**:903–906.
- Hedredya, C. T., K. K. Lee, and D. C. Krause. 1993. Transformation of *Mycoplasma pneumoniae* with Tn4001 by electroporation. *Plasmid* **30**:170–175.
- Hegermann, J., R. Herrmann, and F. Mayer. 2002. Cytoskeletal elements in the bacterium *Mycoplasma pneumoniae*. *Naturwissenschaften* **89**:453–458.
- Himmelreich, R., H. Plagens, H. Hilbert, B. Reiner, and R. Herrmann. 1997. Comparative analysis of the genomes of the bacteria *Mycoplasma pneumoniae* and *Mycoplasma genitalium*. *Nucleic Acids Res.* **25**:701–712.
- Hu, P. C., R. M. Cole, Y. S. Huang, J. A. Graham, D. E. Gardner, A. M. Collier, and W. A. Clyde, Jr. 1982. *Mycoplasma pneumoniae* infection: role of a surface protein in the attachment organelle. *Science* **216**:313–315.
- Inamine, J. M., S. Loechel, and P. C. Hu. 1988. Analysis of the nucleotide sequence of the P1 operon of *Mycoplasma pneumoniae*. *Gene* **73**:175–183.
- Jordan, J. L., K. M. Berry, M. F. Balish, and D. C. Krause. 2001. Stability and subcellular localization of cytodherence-associated protein P65 in *Mycoplasma pneumoniae*. *J. Bacteriol.* **183**:7387–7391.
- Kirchhoff, H. 1992. Motility, p. 473–489. *In* J. Maniloff, R. N. McElhane, L. R. Finch, and J. B. Baseman (ed.), *Mycoplasmas: molecular biology and pathogenesis*. American Society for Microbiology, Washington, D.C.
- Knudtson, K. L., and F. C. Minion. 1993. Construction of Tn4001 derivatives to be used as promoter probe vectors in mycoplasmas. *Gene* **137**:217–222.
- Krause, D. C. 1998. *Mycoplasma pneumoniae* cytodherence: organization and assembly of the attachment organelle. *Trends Microbiol.* **6**:15–18.
- Krause, D. C. 1996. *Mycoplasma pneumoniae* cytodherence: unravelling the tie that binds. *Mol. Microbiol.* **20**:247–253.
- Krause, D. C., and M. F. Balish. 2004. Cellular engineering in a minimal microbe: structure and assembly of the terminal organelle of *Mycoplasma pneumoniae*. *Mol. Microbiol.* **51**:917–924.
- Krause, D. C., and M. F. Balish. 2001. Structure, function, and assembly of the terminal organelle of *Mycoplasma pneumoniae*. *FEMS Microbiol. Lett.* **198**:1–7.
- Krause, D. C., D. K. Leith, R. M. Wilson, and J. B. Baseman. 1982. Identification of *Mycoplasma pneumoniae* proteins associated with hemadsorption and virulence. *Infect. Immun.* **35**:809–817.
- Krause, D. C., T. Proft, C. T. Hedredya, H. Hilbert, H. Plagens, and R. Herrmann. 1997. Transposon mutagenesis reinforces the correlation between *Mycoplasma pneumoniae* cytoskeletal protein HMW2 and cytodherence. *J. Bacteriol.* **179**:2668–2677.
- Layh-Schmitt, G., and R. Herrmann. 1992. Localization and biochemical characterization of the ORF6 gene product of the *Mycoplasma pneumoniae* P1 operon. *Infect. Immun.* **60**:2906–2913.
- Layh-Schmitt, G., A. Podtelejnikov, and M. Mann. 2000. Proteins complexed to the P1 adhesin of *Mycoplasma pneumoniae*. *Microbiology* **146**:741–747.
- Lipman, R. P., W. A. Clyde, Jr., and F. W. Denny. 1969. Characteristics of virulent, attenuated, and avirulent *Mycoplasma pneumoniae* strains. *J. Bacteriol.* **100**:1037–1043.
- McBride, M. J. 2001. Bacterial gliding motility: multiple mechanisms for cell movement over surfaces. *Annu. Rev. Microbiol.* **55**:49–75.
- Meng, K. E., and R. M. Pfister. 1980. Intracellular structures of *Mycoplasma pneumoniae* revealed after membrane removal. *J. Bacteriol.* **144**:390–399.
- Miyata, M. 2002. Cell division, p. 117–130. *In* S. Razin and R. Herrmann (ed.), *Molecular biology and pathogenicity of mycoplasmas*. Kluwer Academic/Plenum Publishers, New York, N.Y.
- Miyata, M., W. S. Ryu, and H. C. Berg. 2002. Force and velocity of *Mycoplasma mobile* gliding. *J. Bacteriol.* **184**:1827–1831.
- Miyata, M., and S. Seto. 1999. Cell reproduction cycle of mycoplasma. *Biochimie* **81**:873–878.
- Miyata, M., and A. Uenoyama. 2002. Movement on the cell surface of the gliding bacterium, *Mycoplasma mobile*, is limited to its head-like structure. *FEMS Microbiol. Lett.* **215**:285–289.
- Miyata, M., H. Yamamoto, T. Shimizu, A. Uenoyama, C. Citti, and R. Rosengarten. 2000. Gliding mutants of *Mycoplasma mobile*: relationships

- between motility and cell morphology, cell adhesion and microcolony formation. *Microbiology* **146**:1311–1320.
39. Phillips, G. J. 2001. Green fluorescent protein—a bright idea for the study of bacterial protein localization. *FEMS Microbiol. Lett.* **204**:9–18.
 40. Proft, T., H. Hilbert, G. Layh-Schmitt, and R. Herrmann. 1995. The proline-rich P65 protein of *Mycoplasma pneumoniae* is a component of the Triton X-100-insoluble fraction and exhibits size polymorphism in the strains M129 and FH. *J. Bacteriol.* **177**:3370–3378.
 41. Proft, T., H. Hilbert, H. Plagens, and R. Herrmann. 1996. The P200 protein of *Mycoplasma pneumoniae* shows common features with the cytodherence-associated proteins HMW1 and HMW3. *Gene* **171**:79–82.
 42. Radestock, U., and W. Brecht. 1977. Motility of *Mycoplasma pneumoniae*. *J. Bacteriol.* **129**:1495–1501.
 43. Razin, S., and E. Jacobs. 1992. Mycoplasma adhesion. *J. Gen. Microbiol.* **138**:407–422.
 44. Razin, S., D. Yogeve, and Y. Naot. 1998. Molecular biology and pathogenicity of mycoplasmas. *Microbiol. Mol. Biol. Rev.* **62**:1094–1156.
 45. Regula, J. T., G. Boguth, A. Gorg, J. Hegermann, F. Mayer, R. Frank, and R. Herrmann. 2001. Defining the mycoplasma 'cytoskeleton': the protein composition of the Triton X-100 insoluble fraction of the bacterium *Mycoplasma pneumoniae* determined by 2-D gel electrophoresis and mass spectrometry. *Microbiology* **147**:1045–1057.
 46. Romero-Arroyo, C. E., J. Jordan, S. J. Peacock, M. J. Willby, M. A. Farmer, and D. C. Krause. 1999. *Mycoplasma pneumoniae* protein P30 is required for cytodherence and associated with proper cell development. *J. Bacteriol.* **181**:1079–1087.
 47. Sambrook, J., and D. W. Russell. 2001. *Molecular cloning: a laboratory manual*, 3rd ed. Cold Spring Harbor Laboratory Press, Cold Spring Harbor, N.Y.
 48. Seto, S., G. Layh-Schmitt, T. Kenri, and M. Miyata. 2001. Visualization of the attachment organelle and cytodherence proteins of *Mycoplasma pneumoniae* by immunofluorescence microscopy. *J. Bacteriol.* **183**:1621–1630.
 49. Seto, S., and M. Miyata. 2003. Attachment organelle formation represented by localization of cytodherence proteins and formation of the electron-dense core in wild-type and mutant strains of *Mycoplasma pneumoniae*. *J. Bacteriol.* **185**:1082–1091.
 50. Southward, C. M., and M. G. Surette. 2002. The dynamic microbe: green fluorescent protein brings bacteria to light. *Mol. Microbiol.* **45**:1191–1196.
 51. Stevens, M. K., and D. C. Krause. 1991. Localization of the *Mycoplasma pneumoniae* cytodherence-accessory proteins HMW1 and HMW4 in the cytoskeletonlike Triton shell. *J. Bacteriol.* **173**:1041–1050.
 52. Willby, M. J., and D. C. Krause. 2002. Characterization of a *Mycoplasma pneumoniae* *hmw3* mutant: implications for attachment organelle assembly. *J. Bacteriol.* **184**:3061–3068.
 53. Yanisch-Perron, C., J. Vieira, and J. Messing. 1985. Improved M13 phage cloning vectors and host strains: nucleotide sequences of the M13mp18 and pUC19 vectors. *Gene* **33**:103–119.

Antigenic Divergence Suggested by Correlation between Antigenic Variation and Pulsed-Field Gel Electrophoresis Profiles of *Bordetella pertussis* Isolates in Japan

Atsuko Kodama,^{1,2} Kazunari Kamachi,^{1*} Yoshinobu Horiuchi,¹ Toshifumi Konda,¹
and Yoshichika Arakawa¹

Department of Bacterial Pathogenesis and Infection Control, National Institute of Infectious Diseases,¹
and Department of Biological Science, Graduate School of Science,
Tokyo Metropolitan University,² Tokyo, Japan

Received 12 April 2004/Returned for modification 28 May 2004/Accepted 9 August 2004

Antigenic divergence has been found between *Bordetella pertussis* vaccine strains and circulating strains in several countries. In the present study, we analyzed *B. pertussis* isolates collected in Japan from 1988 to 2001 using pulsed-field gel electrophoresis (PFGE) and sequencing of two virulence-associated proteins. The 107 isolates were classified into three major groups by PFGE analysis; 87 (81%) were type A, 19 (18%) were type B, and 1 (1%) was type C. Sequence analysis of the S1 subunit of pertussis toxin (*ptxS1*) and adhesion pertactin (*prn*) genes revealed the presence of two (*ptxS1A* and *ptxS1B*) and three (*prn1*, *prn2*, and *prn3*) variants, respectively, in the isolates. Among those isolates, 82 (95%) of the 87 type A strains and the type C strain had the same combination of *ptxS1B* and *prn1* alleles (*ptxS1B/prn1*) as the Japanese vaccine strain. On the other hand, 17 (90%) of 19 type B strains had an allele (*ptxS1A/prn2*) distinct from that of the vaccine strain. A correlation was found between the antigenic variation and the PFGE profile in the isolates. In addition, the frequency of the type B strain was 0, 27, 0, 42, and 37% of the isolates in the periods 1988 to 1993, 1994 to 1995, 1996 to 1997, 1998 to 1999, and 2000 to 2001, respectively. In contrast, the number of reported pertussis-like and pertussis cases decreased gradually from 1991 on, suggesting that the antigenic divergence did not affect the efficacy of pertussis vaccination in Japan.

Bordetella pertussis is the primary etiologic agent of the disease pertussis. Whole-cell and acellular pertussis vaccines have been very effective at inducing protection against *B. pertussis* infection (23, 24). In Japan, pertussis vaccination was started in 1950 using whole-cell vaccine. Then, in 1981, acellular pertussis vaccines containing detoxified pertussis toxin (PT) and filamentous hemagglutinin as major antigens were introduced and have successfully controlled the prevalence of pertussis ever since (24). Most people with cases of pertussis (98.7%) reported to the National Epidemiological Surveillance of Infectious Diseases from 1987 to 1996 had no history of pertussis vaccination in Japan (21). However, in recent years, a resurgence of pertussis has been found in several countries despite high vaccination coverage (1, 5, 8). Since Mooi et al. (20) found that the circulating clinical strains had antigens distinct from those of vaccine strains, they proposed that the circulating clinical strains might have escaped the immunity provided by pertussis vaccination. The antigenic divergence between recently circulating strains and vaccine strains has been reported in European and North American countries (3, 6, 9, 16, 19, 22, 29–31) but not in Asian countries.

In the United States and France, genetic diversity of circulating *B. pertussis* isolates has been observed using pulsed-field gel electrophoresis (PFGE) (10, 31). In addition, the genetic divergence between circulating strains and vaccine strains can

also be detected by DNA typing analyses, by IS1002-based DNA fingerprinting, and by sequencing the structural genes encoding *B. pertussis* virulence factors. The antigenic variants have been observed in the genes encoding the S1 subunit of PT (*ptxS1*) and pertactin (*prn*), which are important virulence factors of *B. pertussis*. Recently, polymorphism was also found in the genes encoding the S3 subunit of PT (*ptxS3*) and tracheal colonization factor (*tcf*) in circulating clinical strains (28). However, it is not clear whether the antigenic variations and DNA types in *B. pertussis* are associated with each other. For example, van Loo et al. (29, 30) found congruence between clustering based on IS1002-based DNA fingerprint types of Dutch clinical strains and the *ptxS1* allele but not the *prn* allele. In contrast, in those strains found recently in France, most of the circulating strains showed a correlation between the PFGE profile and *prn* allele but not *ptxS1* (31). Moreover, there was no high correlation between the PFGE types and the combinations of *ptxS1* and *prn* alleles in the strains found in Canada or the United States (3, 22).

In a previous study, most Japanese *B. pertussis* isolates (83%) collected in the period 1975 to 1996 had the same *ptxS1* and *prn* alleles as the Japanese vaccine strain, whereas the two recently circulating isolates exhibiting a different PFGE profile had *ptxS1* and *prn* alleles different from those of the vaccine strain (7). Since a limited number of isolates ($n = 12$) were used in the study, it was not clear whether the antigenic divergence in *ptxS1* and *prn* alleles has progressed in circulating strains in Japan. In the present study, we collected 107 Japanese clinical isolates, including recently circulating strains, and the antigenic divergence in those strains was investigated using

* Corresponding author. Mailing address: Department of Bacterial Pathogenesis and Infection Control, National Institute of Infectious Diseases, 4-7-1 Gakuen, Musashimurayama City, Tokyo 208-0011, Japan. Phone: 81-42-561-0771. Fax: 81-42-565-3315. E-mail: kamachi@nih.go.jp.

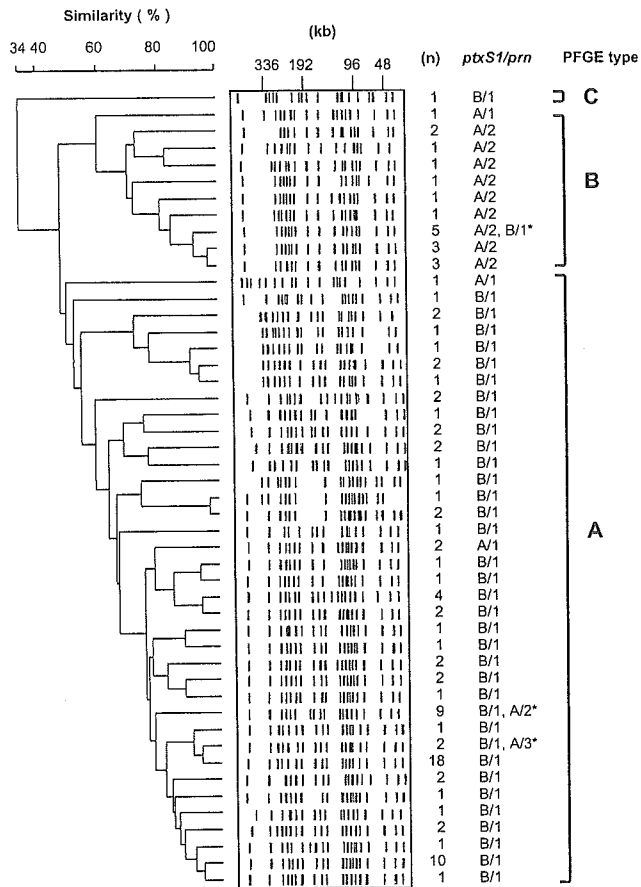


FIG. 1. Dendrogram of PFGE profiles of 107 Japanese *B. pertussis* isolates from 1988 to 2001. The dendrogram was calculated by UP-GMA. The regions including the *ptxS1* and *prn* repeat were sequenced, and the combination of *ptxS1* and *prn* alleles is shown as *ptxS1/prn*, e.g., B/1 indicates *ptxS1B/prn1*. *, one isolate had different *ptxS1/prn* alleles in the PFGE profile.

PFGE analysis and sequencing of *ptxS1* and *prn* alleles. The possible association of the antigenic variations with the PFGE profiles in the isolates was also investigated.

MATERIALS AND METHODS

Isolates. One hundred seven *B. pertussis* clinical isolates, collected from 1988 to 2001 in Japan, were obtained from 22 medical institutes, hospital laboratories, private clinical laboratories, and prefectural public health institutes. The periods of isolation and numbers of strains isolated were as follows: 1988 to 1993, 35; 1994 to 1995, 15; 1996 to 1997, 18; 1998 to 1999, 12; 2000 to 2001, 27. All of the isolates were confirmed as *B. pertussis* in our laboratory using PCR identification (14). For comparison, the Japanese acellular vaccine strain *B. pertussis* Tohama was used as a reference strain. The strains were cultured on Bordet-Gengou agar (Difco) supplemented with 1% glycerol and 15% defibrinated horse blood and incubated at 36°C for 2 to 3 days.

PFGE analysis. PFGE was performed according to standardized recommendations for typing of *B. pertussis* (18), with minor modifications. Chromosomal DNA was digested with the restriction enzyme XbaI, and the digested fragments were separated using a CHEF DR II apparatus (Bio-Rad). Electrophoresis was performed at 6 V/cm at 16°C with the following ramped switch times: block 1, 4 to 8 s for 12 h; block 2, 8 to 50 s for 10 h. The PFGE patterns were analyzed by the unweighted pair-group method with arithmetic averages (UPGMA) using Diversity Database version 1.1 software (PDI, Inc.).

DNA sequencing. DNA sequencing of relevant regions of the pertactin (*prn*) and S1 subunit of pertussis toxin (*ptxS1*) genes was performed on PCR fragments as described previously (18). Chromosomal DNA of *B. pertussis* was isolated

using a QIAGEN genomic tip (20G) and genomic DNA buffer set. Sequence reactions were carried out with a BigDye terminator version 3.1 cycle-sequencing kit (Applied Biosystems), and the products were sequenced on a PRISM 3100 genetic analyzer (Applied Biosystems). Regions 1 of *prn* and *ptxS1* were sequenced for all 107 clinical isolates. On the other hand, region 2 of *prn* was sequenced for 40 of the 107 isolates, since polymorphism has been reported infrequently in the region (19, 20). The carbohydrate recognition domain (fragment A) of the *phaB* gene was also sequenced between positions 3421 and 3837 (17). The sense primer fraAF (5'-CGACATCATCATGGATGCGA-3') and the antisense primer fraAR (5'-TCTGGAAAGGTGCCCTGTTC-3') were used for the sequencing.

Purification of PT variants and analysis of biological activity. Two PT variants, PT-194M and PT-194I, encoded by *ptxS1B* and *ptxS1A*, respectively, were purified from each culture supernatant using an Affi-gel blue column and a fetuin-Sepharose column as described previously (25). The protein concentrations of the purified PT variants were measured by Lowry assay with bovine serum albumin as a standard. The purity of PT-194M and PT-194I was >95%, as estimated by sodium dodecyl sulfate-14% polyacrylamide gel electrophoresis, followed by Coomassie blue R-250 staining. The biological activities of the purified PT variants were determined by the Chinese hamster ovary (CHO) cell-clustering test (13).

RESULTS

PFGE typing and polymorphism in PT-S1 and pertactin. Among 107 *B. pertussis* isolates collected in Japan during the period 1988 to 2001, 48 PFGE profiles were identified (Fig. 1). The 48 PFGE profiles were classified into three major groups using UPGMA; type A comprised 37 PFGE profiles, type B comprised 10 profiles, and type C had one profile. The type A strain was a major group of isolates, since 87 (81%) of the 107 isolates were type A. On the other hand, types B and C were minor groups: 19 isolates (18%) were type B and 1 isolate (1%) was type C. Surprisingly, the type C strain had the same profile as the Japanese vaccine strain, *B. pertussis* Tohama.

The *ptxS1* and *prn* genes of all 107 isolates were sequenced. Two PT-S1 subunit alleles (*ptxS1A* and *ptxS1B*) and three pertactin alleles (*prn1*, *prn2* and *prn3*) were identified among the isolates (Fig. 2). Four *ptxS1* and eight *prn* variants have been

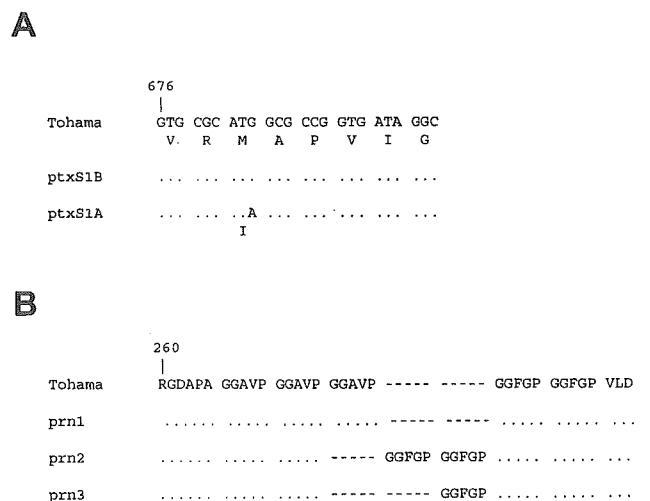


FIG. 2. Variants of pertussis toxin S1 subunit and pertactin observed in Japanese *B. pertussis* isolates. (A) Primary structure of pertussis toxin S1 subunit gene showing regions of polymorphism. (B) Deduced amino acid sequence of region 1 of pertactin. The dots indicate sequence identity with the Japanese vaccine strain, *B. pertussis* Tohama. The dashed lines indicate gaps. The vaccine strain has a combination of *ptxS1B/prn1* alleles.

TABLE 1. Correlation between PFGE type and *ptxS1/prn* alleles in *B. pertussis* isolates collected from 1988 to 2001 in Japan

PFGE type	No. of isolates	No. (%) of <i>ptxS1/prn</i> alleles			
		Old <i>ptxS1B/prn1</i>	Transitional <i>ptxS1A/prn1</i>	New	
				<i>ptxS1A/prn2</i>	<i>ptxS1A/prn3</i>
A	87	82 (95)	3 (3)	1 (1)	1 (1)
B	19	1 (5)	1 (5)	17 (90)	
C	1	1			
Total	107	84 (78)	4 (4)	18 (17)	1 (1)

described (6); however, only two *ptxS1* and three *prn* variants were found in the Japanese isolates. The Japanese vaccine strain had the *ptxS1B* and *prn1* alleles described previously (2, 7). The *fhaB* genes from the 40 selected isolates (type A, 20 isolates; type B, 19 isolates; type C, 1 isolate) were sequenced between bases 3421 and 3837. No polymorphism was observed in the sequence.

Correlation between PFGE type and combination of *ptxS1* and *prn* alleles. As shown in Fig. 1, there was a correlation between the PFGE profile and the combination of *ptxS1* and *prn* alleles in the Japanese isolates, although the smallest genetic distance (10%) was observed between the type A and type B groups. Table 1 summarizes the correlation between the PFGE type and the combination of *ptxS1* and *prn* alleles. For convenience, *ptxS1* and *prn* alleles have been placed in one of three groups: *ptxS1B/prn1*, old; *ptxS1A/prn1*, transitional; and *ptxS1A/prn2* and *ptxS1A/prn3*, new (3, 22). Of the 87 type A strains, 82 (95%) isolates had old *ptxS1B/prn1* alleles and 3 and 2 isolates had transitional and new alleles, respectively. The Japanese vaccine strain also had the old *ptxS1B/prn1*. In contrast, 17 (90%) of 19 type B strains had new *ptxS1A/prn2* alleles, and each isolate had old and transitional alleles.

We also analyzed the PFGE data using the neighbor-joining clustering method instead of UPGMA. All of the type B strains were classified in the same group, and the same result was obtained (data not shown).

Trend in type B strain in Japan. As shown in Fig. 3, type B strains were collected in various areas of Japan, as were type A strains. Four type B strains were first collected in the Chugoku and Hokkaido districts in 1994 and 1995. Five were collected consecutively in the Kinki and Kanto districts in 1998 and 1999, and 10 were collected in the Tohoku, Kanto, and Kinki districts in 2000 and 2001 (data not shown). Thus, type B strains were widely distributed throughout Japan during these times.

Figure 4B shows the temporal trend of the frequency of the type B strain according to the year of collection. Surprisingly, the percentage of the type B strain changed between 1994 and 1995 and between 2000 and 2001 (0% from 1988 to 1993, 27% from 1994 to 1995, 0% from 1996 to 1997, 42% from 1998 to 1999, and 37% from 2000 to 2001), although the numbers of reported pertussis-like and pertussis cases had decreased gradually from 1991 (Fig. 4A). The temporal trend of the type B strain harboring new *ptxS1A/prn2* was the same as the trend of the type B strain. The frequency of the type B strain harboring *ptxS1A/prn2* was 20, 0, 42, and 33% of the isolates in the periods 1994 to 1995, 1996 to 1997, 1998 to 1999, and 2000 to 2001, respectively.

Biological activities of PT variants. The biological activities of vaccine-type PT (PT-194M) and nonvaccine-type PT (PT-194I) were assessed. Two PT variants, PT-194M and PT-194I, encoded by the old *ptxS1B* and the new *ptxS1A*, respectively, were purified from each culture supernatant, and the biological activities of the purified PT variants were determined by the CHO cell-clustering test. The minimum concentrations required for the clustering of PT-194M and PT-194I were assessed to be 68 (95% confidence interval, 52 to 89) and 44 pg/ml (95% confidence interval, 25 to 76 pg/ml), respectively. No significant difference was observed between the biological activities.

DISCUSSION

In a previous study, most Japanese *B. pertussis* isolates collected from 1975 to 1996 had the same *ptxS1B* and *prn1* alleles as the Japanese vaccine strain (7). However, since a limited number of isolates were used in the study, it was not clear whether the antigenic divergence between recently circulating strains and the vaccine strain has progressed. In the present study, 107 Japanese *B. pertussis* isolates, including recently circulating strains, were collected, and the antigenic divergence in those isolates was investigated. We found that the type B

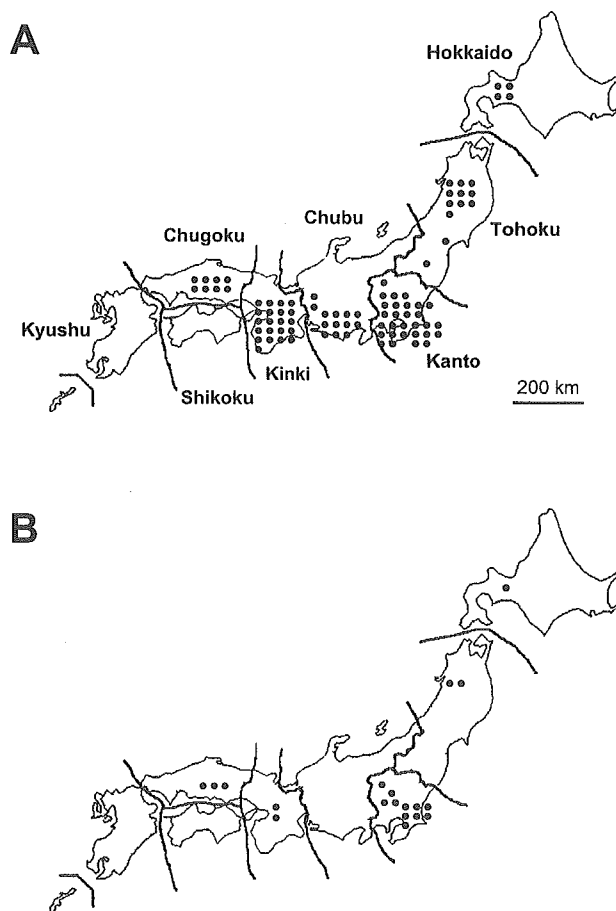


FIG. 3. Geographic distribution of type A (A) and type B (B) strains collected from 1988 to 2001 in Japan. The numbers of symbols indicate the numbers of isolates.

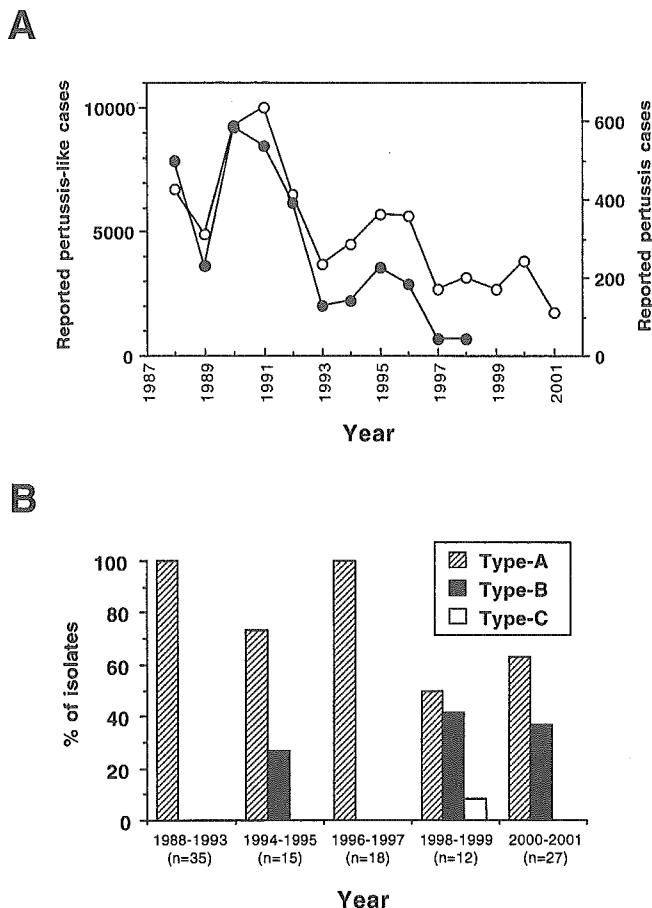


FIG. 4. Temporal trend in isolation of type B strains and reported pertussis cases in Japan. (A) Pertussis-like cases (○) and pertussis cases (●) reported by sentinel clinics and hospitals in Japan from 1988 to 2001. The data were obtained from Infectious Disease Surveillance data of the Ministry of Health, Labor and Welfare of Japan. The reporting of pertussis cases was discontinued in 1999. (B) Changes in the frequencies of type A, type B, and type C strains.

strain harboring nonvaccine *ptxS1A* and *prn2* alleles appeared during the period 1994 to 1995. Thus, the antigenic divergence has progressed since the mid-1990s in Japan, similar to other countries, such as European and North American countries.

Despite high vaccination coverage, the resurgence of pertussis has been reported in several countries (1, 5, 8). In The Netherlands, the incidence of pertussis increased dramatically in 1996 and 1997 (5), and the antigenic divergence in the protective antigens encoded by *ptxS1* and *prn* was observed in the circulating strains (20). In regard to the resurgence, Mooi et al. (20) proposed that circulating strains distinct from the vaccine strain might have escaped the immunity provided by vaccination. In contrast, in the United Kingdom, an antigenic divergence in the *prn* allele was observed in recently circulating strains (6), despite the relatively few pertussis cases there (27). These observations suggested that the presence of nonvaccine *prn2* has not been associated with a resurgence of pertussis. In the present study, the type B strain harboring *ptxS1A/prn2* distinct from those of the vaccine strain appeared in the mid-1990s, although the reported pertussis and pertussis-like cases had decreased since 1991 (Fig. 4). Most type B strains (90%) had not only *prn2* but also nonvaccine *ptxS1A*. Therefore, our

finding suggested that (i) the presence of nonvaccine *ptxS1A*, as with *prn2*, has not been associated with a resurgence of pertussis and (ii) the type B strain might not have escaped the immunity provided by vaccination in Japan.

In a previous study, Weber et al. (31) found no correlation between the PFGE type and the *ptxS1* allele in French *B. pertussis* isolates but revealed a correlation with the *prn* allele. In the Canadian and U.S. isolates, there was no high correlation between the PFGE type and the combination of *ptxS1* and *prn* alleles (3, 22). However, among the U.S. isolates, all isolates harboring *ptxS1A/prn2* clustered in a relatedness group at the phylogenetic tree, whereas isolates harboring *ptxS1B/prn1* and *ptxS1A/prn1* were scattered throughout the tree (3). In contrast, among Japanese isolates, most (90%) type B strains had a combination of *ptxS1A* and *prn2* (*ptxS1A/prn2*) and most (95%) type A strains and the type C strain had the same *ptxS1B/prn1* as the Japanese vaccine strain (Table 1). Thus, there was a correlation between the PFGE types and *ptxS1/prn* alleles in the Japanese isolates. Strains harboring *ptxS1B* and *prn1* had been collected prior to the 1970s in European countries and the United States, whereas strains harboring *ptxS1A*, *prn2*, and *prn3* had been collected in those countries since the early 1980s (3, 19, 20). Therefore, *ptxS1B* and *prn1* alleles have been called old alleles, while *ptxS1A*, *prn2*, and *prn3* are called new alleles (3, 22). Moreover, strains harboring a combination of new and old alleles (*ptxS1A/prn1*) have been called transitional strains. Among strains collected in the United States from 1935 to 1999, 34 (22%) of 152 isolates were transitional strains (3). Similarly, among strains collected in Canada from 1985 to 1994, 17% of the isolates were transitional strains (22). These observations suggested that the *B. pertussis* strain had evolved from an old strain into a new strain by selective pressure from vaccination. However, only four transitional strains (4%) were found among the 107 Japanese isolates in this study. This finding strongly suggested that there was no genetic relationship between old strains (type A and type C) and the new strain (type B), i.e., the type B strain did not derive from the type A or type C strain genetically. One possible explanation for the appearance of the type B strain is that it was imported to Japan from other countries.

Among recently circulating strains in The Netherlands, polymorphism was observed only in *prn*, *ptxS1*, *ptxS3*, and *tcfA* by sequencing 15 genes coding for surface proteins (28). Polymorphism in *prn* is essentially limited to region 1, which has an important role in immunity (12, 15). However, Boursaux-Eude et al. (2) showed that acellular vaccine was highly effective against *B. pertussis* strains harboring nonvaccine *ptxS1* and *prn* alleles by using a mouse intranasal challenge model. On the other hand, Hausman and Burns (11) suggested that significant amino acid changes could occur in PT sequence without affecting antibody neutralization. Thus, polymorphism in pertussis toxin may have no influence on the efficacy of antibody neutralization. In the present study, we also investigated the virulence of two PT variants, PT-194 M, encoded by vaccine *ptxS1B*, and PT194I, encoded by nonvaccine *ptxS1A*, but no significant difference between their biological activities was detected. These findings suggested that the virulence of PT-194I had not been associated with the wide spread of the type B strain harboring *ptxS1A/prn2*. The type B strain may have a more important virulent allele(s) than the *ptxS1A* and *prn2*